Assessment of Very High Energy Electron therapy as a clinical modality for external beam therapy

J. Dijkstra

TU Delft

Assessment of Very High Energy Electron therapy as a clinical modality for external beam therapy

by

J. Dijkstra

to obtain the degree of Master of Science
at the Delft University of Technology,

Student number:	4296001	
Project duration:	August, 2019 – July, 2020	
Thesis committee:	Dr. ir. D. Lathouwers,	TU Delft, supervisor
	Prof. dr. B. J. M. Heijmen,	Erasmus MC, supervisor
	Dr. Z Perkó,	TU Delft
	Dr. ir. M. C. Goorden,	TU Delft

An electronic version of this thesis is available at `http://repository.tudelft.nl/`.

TU Delft

Abstract

Purpose: Very high energy electron (VHEE) radiotherapy is being investigated as a potential replacement of photon therapy. VHEE pencil beams have a small penumbra and strong depth dependence for radiotherapy when compared to photons. This allows a lower dose to healthy tissue. Generating these high electron energy beams could be achieved by using laser accelerators. These accelerators allow the equipment to be smaller than currently possible and make it possible to fit them in a standard radiotherapy treatment bunker. This makes VHEE a potential middle ground between photon and proton therapy in relation to equipment costs and treatment quality. The purpose of this project is to compare photon based Intensity Modulated Radiation Therapy (IMRT) and VHEE treatment plans for treatment of prostate cancer.
Method: For 10 prostate cancer patients IMRT treatment plans were generated with 23 beams. These plans were optimized using Erasmus MC in-house developed Erasmus-iCycle automated treatment plan optimization tool. The dependence of VHEE plan quality on beam energy (200, 300 and 400 MeV) and number of equi-angular beams (9, 18 and 36) was investigated. The treatment plans were optimized using the multi-criterial optimizer Erasmus-iCycle. For each patient VHEE pencil beam dose distributions were pre-calculated using TOPAS MC, a Monte Carlo simulation program based on Geant4.
Results: VHEE treatment plans show either a reduced or similar mean OAR dose when compared to IMRT treatment plans except for the 9 beam 200 MeV plan which was worse compared to IMRT. All treatment plans were normalized to a PTV coverage of 99% V_{57Gy}.

It is found that the mean rectum dose reduces from 13.5 Gy for IMRT to between 9.2 and 11.9 (p=0.002-0.004) for the VHEE plans. For the anus dose a reduction in mean dose was found for all VHEE treatment plans except for the 9 beam 200 MeV and the 18 beam 200 MeV VHEE treatment plans. The mean anus dose reduced from 12.4 Gy for IMRT to 7.0 - 10.6 Gy (p=0.002-0.014) for the VHEE treatment plans. The bladder dose reduced from 20.1 Gy to between 15.2 and 18.2 Gy (p=0.002).

Increasing the number of VHEE beams in a treatment plan reduces the OAR dose. Comparing 9, 18 and 36 beam treatment plans with 300 MeV. The mean rectum dose reduces from 14.0 Gy for the 9 beam plan to 11.1 Gy (p=0.002) and 9.9 Gy (p=0.002) for the 18 and 36 beam plan, respectively. The same pattern is found for the anus and bladder.

Treatment plans with a higher beam energy reduces the dose to OAR. The mean rectum dose reduces from 13.4 Gy for the 200 MeV plan to 11.1 (p=0.002) and 10.0 (p=0.002) Gy for the 300 and 400 MeV plans. The same pattern is found in the mean bladder dose with 18.2 Gy, 16.8 Gy (p=0.002) and 15.9 Gy (p=0.002). The right femoral head maximum dose increases from 28.0 Gy for 200 MeV to 29.4 Gy(p=0.002) and 29.6 Gy (p=0.049) for the 300 and 400 MeV treatment plans.
Conclusion: VHEE is a potential replacement for IMRT due to the reduced dose to healthy tissue while maintaining similar target coverage compared to IMRT. By increasing the number of beams and/or the electron beam energy we can further reduce doses to the healthy tissue.

Contents

1 Introduction **1**

2 Background **3**
2.1 Radiotherapy . . . 3
2.2 Tissue response to radiation . . . 4
2.3 Particle interactions in matter . . . 6
2.3.1 Photon interactions . . . 6
2.3.2 Electron interactions . . . 7
2.4 Electron beam characteristics . . . 8
2.4.1 Penumbra . . . 8
2.4.2 Percentage depth dose . . . 9
2.4.3 lateral distribution . . . 10
2.5 Monte Carlo Simulations . . . 11
2.6 Treatment plan optimization . . . 12

3 Literature Study VHEE **13**
3.1 Beam characteristics . . . 14
3.1.1 Experimental . . . 14
3.1.2 Monte Carlo simulations . . . 17
3.2 Radiotherapy plans . . . 21
3.3 Conclusion literature study . . . 24

4 Materials and Methods **25**
4.1 Patients . . . 25
4.2 Workflow . . . 25
4.3 Monte Carlo dose calculations . . . 26
4.3.1 Pencil beam generation . . . 26
4.3.2 TOPAS MC output . . . 28
4.4 Optimization of treatment plans . . . 28
4.4.1 Plan generation . . . 29
4.4.2 Automated generation 23-beam IMRT plans . . . 29
4.4.3 Plan quality evaluations . . . 29

5 Results **31**
5.1 Comparing treatment plans with 9, 18 and 36 beams . . . 31
5.2 Comparing treatment plans with 200,300 and 400 MeV . . . 36
5.3 Combined 200/300 MeV Treatment plan . . . 41
5.4 Computational performance . . . 42

6 Discussion **43**
6.1 Comparison of VHEE and IMRT treatment plans . . . 43
6.2 Influence of the number of beams . . . 44
6.3 Influence of the electron beam energy . . . 44
6.4 Further work . . . 44

Appendices **47**

A Workflow VHEE **49**

B Wishlist iCycle **51**

C TOPAS pencil beam **53**

D TOPAS main code **55**

E 300 MeV treatment plans per patient for 9,18 and 36 beams **59**

F 18 beam plans per patient for 200,300 and 400 MeV **61**

G Table of dosimetric values **63**

Bibliography **67**

1 Introduction

Radiotherapy can be used to control and treat malignant cells (tumor cells) within the human body. The goal of radiotherapy is to deliver a set amount of radiation to the malignant cells while minimizing radiation to healthy tissue. Half of all cancer patients are expected to receive radiotherapy during the course of their treatment [18]. Typically radiotherapy is used in conjunction with other treatment modalities such as surgery and chemotherapy.

Patients can either be treated by insertion of a radioactive source directly into the tumor tissue (brachytherapy) or by external beam radiation. The latter being the focus of this thesis. Treatment planning requires computer tomography (CT) images. These images are used for correction of tissue inhomogeneities in the beam path and to determine the location of the tumor and possible organs at risk (OAR). The OAR are specific volumes within the beam path that have restrictions to the amount of radiation they are allowed to receive. After determining the location of the tumor and the OAR a treatment plan can be created by medical specialists. The plan specifies among other things the modality, beam characteristics, beam angles/modulation and treatment times.

In Figure 1.1 a dose distribution superimposed on a CT cross-section is shown. By combining multiple beams it is possible to obtain high dose inside the tumor and limiting the dose to healthy tissue. Radiotherapy is typically delivered using a Linear Accelerator (LINAC) in a therapy bunker such as shown in Figure 1.2.

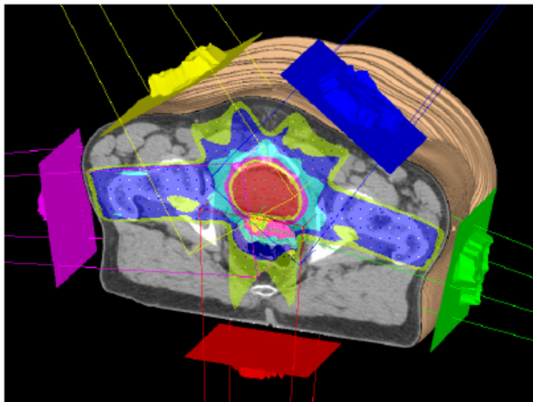

Figure 1.1: 3D rendering radiotherapy treatment plan with 5 beams (yellow,blue,green,red,magenta) and dose distribution with isodose levels. Figure from: Advanced Oncology Center, Inc.

Figure 1.2: Radiotherapy using a linear accelerator (LINAC). Image from: Science Photo Library.

The most common form of external beam radiotherapy uses photon radiation with photon energies in the range of $6 - 15$ MV [39]. Other clinical modalities for radiotherapy are proton therapy and electron therapy. An important characteristic to consider is the percentage depth dose (PDD). This describes the dose deposition in tissue at a certain depth in the body. In Figure 1.3 this metric is shown for photons,

protons and electrons for their integrated dose depth. Photons deposit their dose over a large volume with the peak a few centimeters below the surface.

The depth dose curve of proton beams has a characteristic shape which allows for deposition of a high percentage of its dose at a specific depth. This is called the Bragg peak. By means of range modulation it is possible to move the Bragg peak to a specific position and deposit the dose within the tumor. This allows for a high tumor dose and relative low healthy tissue dose when compared to photon and electron beams. There are two main downsides to proton therapy. The first one is that it requires large and expensive equipment. The second downside is that proton beams are susceptible to heterogeneity of matter. This can cause the Bragg peaks position to easily shift if the patient moves or the matter composition changes, for example due to an gas pocket in the intestines.

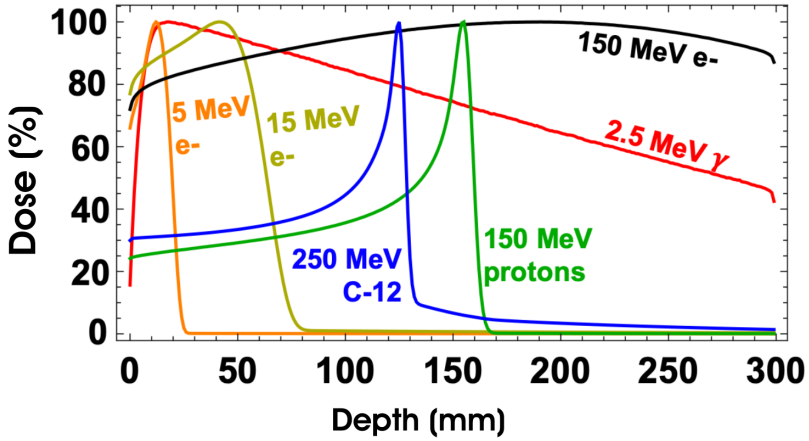

Figure 1.3: Normalized integrated percentage depth dose for $\sigma = 5$ mm pencil beams for photons (red), protons (green), electrons (orange/yellow/black) and carbon ions (blue). Figure from: Lagzda [22].

Electrons are predominantly used for superficial treatment due to a limited penetration depth at energy levels similar to photons. Figure 1.3 shows this lack of dose deposition at depths beyond 10 centimeter. The electrons in question have an energy of up to 50 MeV due to the constraints of clinical linear accelerators (LINAC). If the energy is increased beyond 100 MeV the dose depth curve flattens and extends to greater depths [11]. These high energy electrons are called very high energy electrons (VHEE). Beside an extended range the VHEE beam results in a smaller penumbra. Penumbra being a measure for how well defined the beam is. We could use these VHEE beams for treatment of deep-seated tumors. The downside of using electrons for deep-seated tumors is a high entrance dose to the skin.

Currently VHEE beams are not used in a clinical setting. Accelerating electrons beyond 100 MeV requires large setups and exist only at research facilities such as the SPARC LINAC (INFN, Italy). In recent years test have been performed with smaller setups such as the ALPHA-X laser setup [41]. These new setups could be made small enough to be placed in a traditional therapy bunker. This would reduce the costs associated with VHEE therapy while potentially providing a better treatment when compared to photon therapy.

The purpose of this project is to compare radiotherapy VHEE and IMRT treatment for prostate cancer patients. The IMRT treatment plans are 23 beam and designed to simulate VMAT plans. Systematic investigations on the dependence of VHEE plan quality on applied beam energy (200, 300 and 400 MeV) and number of equi-angular beams (9, 18 and 36). The plans were automatically generated with the Erasmus-iCycle multi-criterial optimizer. For each patient VHEE pencil beam dose distributions were pre-calculated using TOPAS MC. Optimal intensities were established with Erasmus-iCycle treatment plan optimization.

In this thesis the basics of particle interactions, Monte Carlo simulations and treatment plan optimizations will be explained in the background chapter. The method section will describe the used methodology during the Monte Carlo simulations and optimization. The last three chapters are the results, discussion and conclusion.

2

Background

This chapter will provide background information on radiotherapy, Monte Carlo simulations and treatment plan optimizations. These are key components in the process of simulating and optimizing a radiotherapy plan. We start with the basic principles of radiotherapy. In the next section the effects of radiation on cell/tissue is explained. Section 2.3 describes particle interactions, Section 2.4 characterizes the important variables of high energy electron pencil beams, Section 2.5 describes the principles of Monte Carlo simulations and the final section describes the working principles of automated treatment plan optimization.

2.1. Radiotherapy

It is important to minimize radiation to healthy tissues in order to avoid or reduce side effects. The extent of the side effects depends on the location of the tumor within the body, the amount of radiation, treatment method and the patient characteristics. Side effects can be caused directly due to DNA damage or indirectly due to damaged blood vessels or connective tissue. DNA damage can in turn result in new malignant cells.

Reduction of radiation to healthy tissue can be achieved by using multiple angles of irradiation, fractionation and modulation of the beam. By using multiple beam angles we can irradiate the tumor up to the required dose, while keeping the dose to healthy tissue low. The dose to healthy tissue will be lower but spread out over a large area.

Fractionation takes advantage of the fact that healthy cells have a higher recovery rate when compared to malignant cells. By administering a low dose of 2-3 Gy repeatedly over 20-30 fractions, the normal cells will recover more quickly than the tumor cells between fractions.

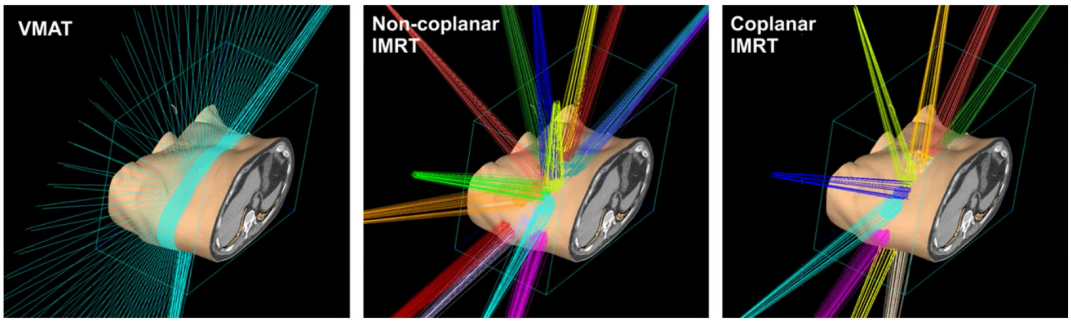

Figure 2.1: Beam setup for VMAT, non-coplanar IMRT and coplanar IMRT treatment plans. Figure from: Holt et al. [17].

The tumour irradiation should result in a homogeneous dose, while maintaining a conformal dose distribution, in other words we are looking for a uniform dose within the target at the prescribed level while keeping the dose outside of the tumor as low as possible. Modulation of the beam allows us to achieve a more conformal dose distribution.

We can achieve this modulation by reshaping the beam for each angle. Intensity Modulated Radiation Therapy (IMRT) achieves this by controlling the intensity of the beam. If we apply the dose continuously over an arc it is called Volumetric Modulated Arc therapy (VMAT). If we only allow beams to target the patient in the transverse plane we call the therapy coplanar. This is shown in panel one and three for VMAT and IMRT in Figure 2.1. The second panel shows non-coplanar therapy. Non-coplanar has the benefit of reducing overlap between beams and so reduces healthy tissue damage, but this does increase the required computational power.

VMAT and IMRT both use collimators for beam shaping. This allows for a high conformal dose to be delivered to the target. The beams for VMAT and IMRT are generated using passive scattering. As shown in the top of Figure 2.2. A more precise but time consuming method is pencil beam scanning also called active scanning, see bottom of Figure 2.2. pencil beam scanning uses a small millimeter lateral distribution beam. The beam is steered across the target using electro-magnets. Modulation is achieved by variation of beam time for each pencil beam.

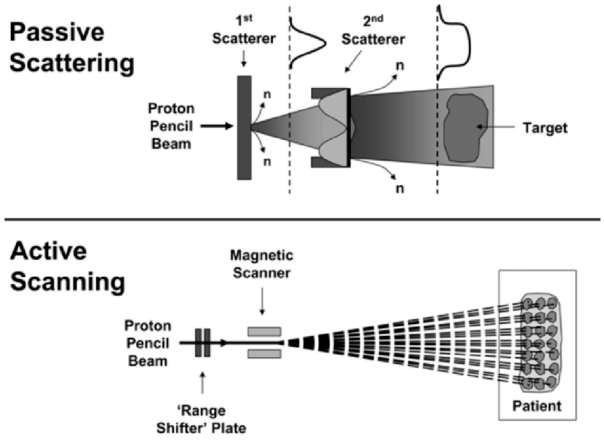

Figure 2.2: Top figure: Passive scattering resulting in a broad beam for proton therapy. Bottom figure: Active scanning or pencil beam scanning spot wise irradiation using pencil beams. Figure from: Leroy et al. [24].

2.2. Tissue response to radiation

Radiation due to radiotherapy can cause cell death and cell mutations. Mapping of damage is impossible because radiation damage occurs on an atomic level, but can result in biological effect within complete biological systems. The damage is (believed to be) caused by direct damage to DNA or indirectly by creating radicals e.g. reactive oxygen species (ROS), hydroxyl radical (OH) and ionized water (H_2O+) as shown in Figure 2.3. The indirectly generated radicals can cause cell damage at the location of creation. If the radicals are soluble they can travel to neighboring cells and cause damage there [22, 37].

After the cell has been damaged the cell either repairs the damage, dies from the damage or the cell is repaired but is non-identical to before the radiation damage. Non-identical repair can cause the cell to develop into a new malignant tumor cell.

The likelihood of a cell being damaged and subsequently being able to repair depends on a large number of variables e.g. cell type, oxygenation, cell division stage, the patients' health and genes. Currently we are not able to predict the effects of irradiation to a specific cell, so we are required to use models to estimate the expected effects on a macro level [37].

To model biological effects the linear-quadratic TCP/NTCP model is a common choice. The model is believed to be a good descriptor of experimental settings, but a relative large uncertainty is contained within the model [19].

The tumor control probability (TCP) describes the probability that no tumor cell survives. For this we use the following formulas.

$$TCP = e^{-N \cdot p_s(D)} \tag{2.1}$$

N is the number of initial tumor cells and $p_s(D)$ cell survival fraction for a dose D. Cell survival after the irradiation is described by $p_s(D)$.

$$p_s(D) = e^{-\alpha D - \beta D^2} \tag{2.2}$$

We can describe $p_s(D)$ by the linear quadratic model as shown above. $p_s(D)$ is the surviving fraction of cells after a dose D. α and β are the cell radiosensitivy coefficients. These values are not known for individual patients. Clinical knowledge does exist about α/β.

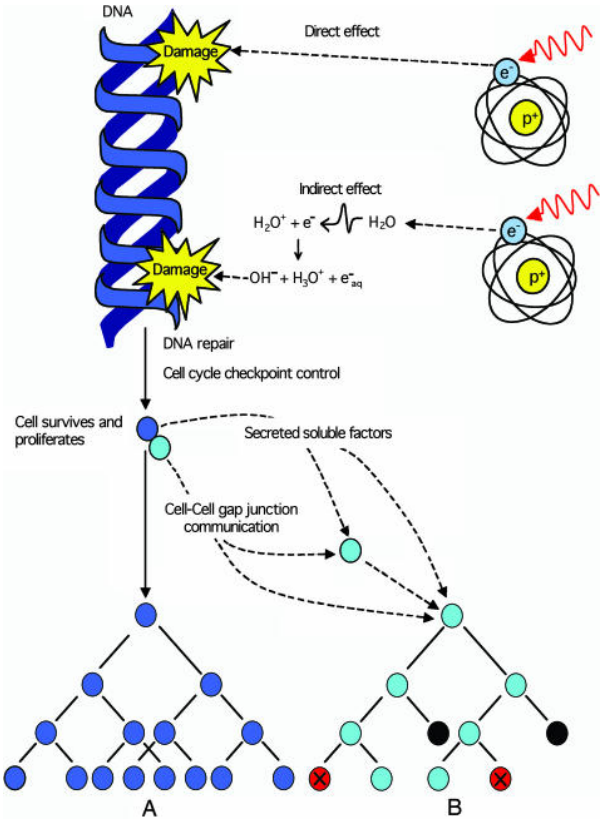

Figure 2.3: Direct and indirect DNA damage due to ionizing radiation. A) Cell (blue)survives and proliferates or due to cell damage apoptosis might occur. B) If the blue cells can communicate with non-irradiated neighboring cells (cyan) by cell-to-cell gap junction communication and/or secretion of soluble factors cell apoptosis (black) or micronucleation (red) can occur in cells that have never been exposed to radiation. Figure from: Morgan and Sowa [30].

Normal Tissue Complication Probability (NTCP) describes the probability of complications in normal tissue due to treatment. A common model for NTCP is the Lyman Kutcher Burman (LKB) model:

$$NTCP = \frac{1}{\sqrt{2\pi}} \int_{-\infty}^{t} e^{-x^2/2} dx \tag{2.3}$$

$$t = \frac{gEUD - TD_{50}}{mxTD_{50}} \tag{2.4}$$

$$gEUD = \left(\sum_i v_i d_i^{1/n} \right)^n \tag{2.5}$$

Here gEUD is the generalized equivalent uniform dose with the i^{th} bin of the DVH having a dose d_i and a relative volume v_i.

TD_{50} is the tolerance dose which results in complications for 50% of the patients and m the steepness of the NTCP curve. The n, m and TD_{50} are complication specific.

In Figure 2.4 we can see the probability of complications for both the tumour (blue) and normal tissue (red). The two are seperated in this gap the normal tissue complication probability is considerably lower compared to the probability of damaging the tumor cells, this region is called the therapeutic window.

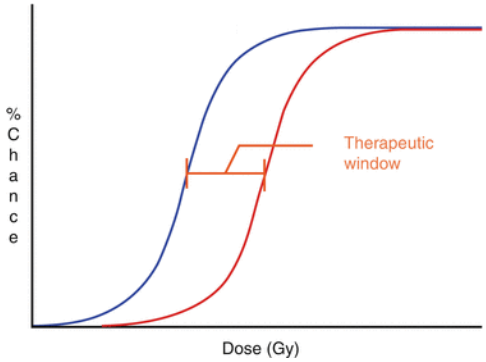

Figure 2.4: Therapeutic window between tumor control (blue) and Normal Tissue Complication (red). Figure from: Chang et al. [9].

2.3. Particle interactions in matter

Photon, proton and electron irradiation can lead to tissue damage in different ways. In this section only the most relevant particle interactions are described. Although it should be noted interactions of elementary particles with matter at high energies can result in a wide variety of outcomes (e.g. proton beams can cause secondary neutrons [11, 38]). In this section we will discuss photon interactions, charged particle interactions and heavy charged particle interactions.

2.3.1. Photon interactions

Photons are non-ionizing particles mostly interacting with the orbital electrons of particles. There are three main effects; the photo-electric effect; Compton scattering and pair production. Figure 2.5 shows the attenuation coefficient for photons in water.

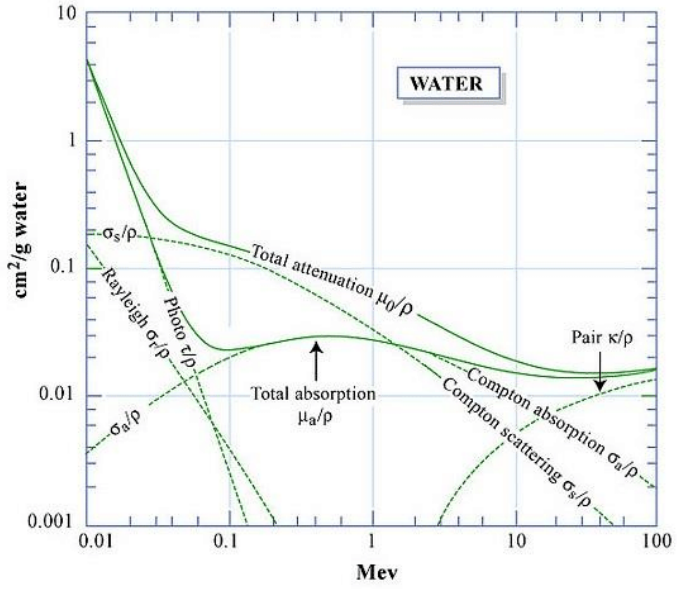

Figure 2.5: Mass attenuation coefficients for photons in water (source: MIT OpenCourseWare - 22.101 Applied Nuclear Physics, Fall 2006)

The photoelectric effect is the dominant effect at lower particle energies (up to about 1 MeV). Absorption

of the photon results in the emission of an electron. The electron will have the photon energy minus the binding energy to the atom.

Compton scattering is an inelastic scattering typically with an electron. This results in transfer of energy and change of momentum for the photon. In the low energy limit of Compton scattering there is no energy transfer, this is called Thomson scattering.

The last major interaction method is pair production. If the photon has at least 1.022 MeV (twice the rest energy of an electron) the photon can convert into an electron-positron pair.
Photons that are used for radiotherapy are generated by impacting an electron beam on a high Z value material. These photons have an energy in the range of 6-20 MeV.

$$I(x) = I_0 \cdot e^{-\mu x} \tag{2.6}$$

With I the intensity at depth x, I_0 the initial beam intensity and μ the attenuation coefficient. The μ characterizes the probability of interactions with matter.

2.3.2. Electron interactions

Charged particles such as electrons directly interact with matter. This happens by Coulomb interactions with orbital electrons and the nuclei. The most relevant interactions are ionizations of atom, excitations of atom and bremsstrahlung.

Ionization of an atom is the primary mechanism for electrons to energy loss. An inelastic collision excites an orbital electron. The energy transfer that follows exceeds the binding energy of an orbital electron. This causes the electron to leave the atom's orbit. This electron is a so called secondary electron and is shown in Figure 2.6. If this electron has sufficient energy to cause an other ionization it is called a delta ray (instead of a secondary electron). After the ionization of an atom we have an ion pair, the secondary electron being the negative part and the atom the positively charged ion.

If the electron moves to a higher orbit, instead of leaving the atom, we speak of an excitation of an atom. This state is instable and will lead to de-excitation of the electron and in this process a photon will be emitted.

Bremsstrahlung is caused when the electron is deflected by the nucleus. This is shown in Figure 2.6 B. The electron emits a Bremsstrahlung photon as it decelerates. This is shown in Figure 2.7. A 100 MeV electron in water will loss 50% of its energy by Bremsstrahlung [5].

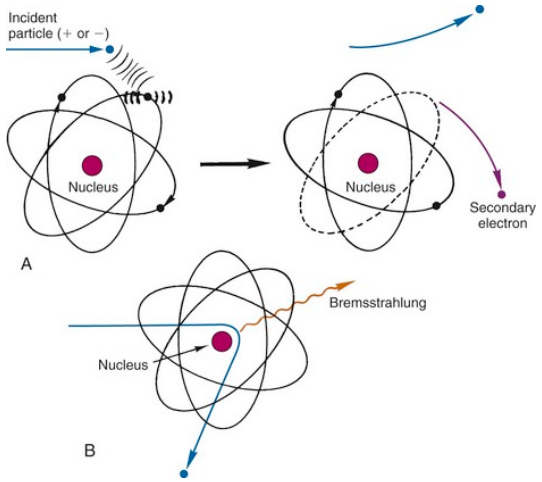

Figure 2.6: Blue line shows trajectory of incident particle. A) Ionization of atom is shown. The incident particle interacting with orbital electron resulting in the deflection of the incident particle and expulsion of secondary electron. B) Bremsstrahlung with the incident particles emitting a bremsstrahlung photon. Figure from: Podgoršak [36]

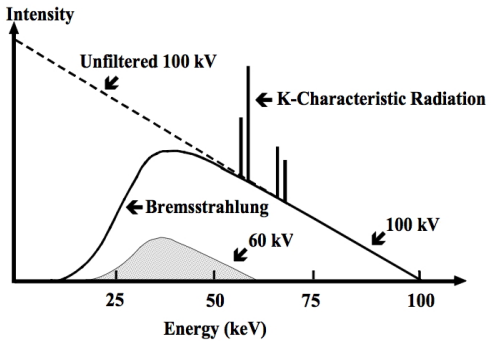

Figure 2.7: Photon spectrum produced by bremsstrahlung. Shown is the intensity of the emitted bremsstrahlung and the energy in keV. Data shown for 100 keV and 60 keV electrons. Figure from: Heggie et al. [16].

Stopping power S is defined as the amount of kinetic energy E lost while traveling a distance dx through matter:

$$S(E) = -\frac{dE}{dx} \tag{2.7}$$

In Figure 2.8 the stopping power for electrons in water is shown. The stopping power consists of collisional and radiative stopping powers. Collisional S are the ionization/excitation of the atoms and the radiative S refers to bremsstrahlung. Figure 2.8 shows that radiative S is dominant at high energies and collisional S at lower energies.
S relates to the mean range R of the particle with E_0 the initial kinetic energy.

$$R = \int_0^{E_0} \frac{1}{S(E)} dE \tag{2.8}$$

For this project we use electrons with energies beyond 100 MeV. Figure 2.8 shows that the electrons initially will be stopped mainly due to Bremsstrahlung. After losing energy inelastic collisions will be the dominated interaction. Figure 2.9 shows a models of stopping power as well as experimentally obtained data. The maximum stopping power for electrons in water is around 0.1 MeV while at about 1 GeV a minimum stopping power is found.

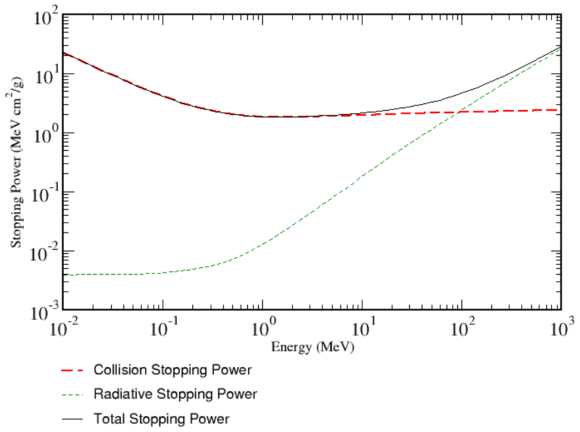

Figure 2.8: Calculated stopping power electrons in water for energies between 10^{-2} to 10^{3} for (red) collision stopping power, (green) radiative stopping power and (black) total stopping power. Figure from: Berger et al. [5].

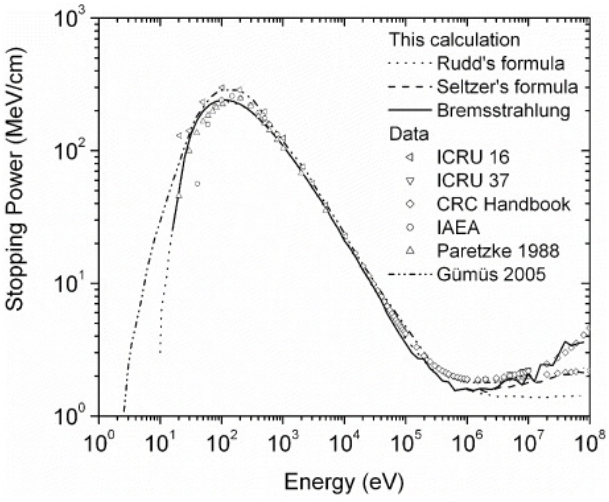

Figure 2.9: Stopping power electrons in water. Figure contains analytical calculations using formula's from Plante and Cucinotta [34] and scientific data. CRC handbook shows total stopping power, while the other data points exclude bremsstrahlung. Figure from: Plante and Cucinotta [34].

2.4. Electron beam characteristics

The previous section discussed the interactions of a single electron with matter. In this section the properties of electron beams with a large number of particles will be examined. We will look at the penumbra, percentage depth dose (PDD) and lateral distribution.

2.4.1. Penumbra

The dose profile in 2D is shown in Figure 2.11 for a 100 MeV electron beam irradiating a water tank. In Figure 2.10 a 1D dose profile of an 100 MeV electron beam is shown. We are looking at the dose perpendicular to the beams propagation direction. A horizontal line in Figure 2.11 will result in a 1D dose profile like we see in Figure 2.10. The dose profile shows in red the ideal dose profile. Due to scattering we can not expect such a profile. Instead we will find a profile close to the black line. The penumbra is defined as the width of the 20 - 80 % intensity region. In the figure this is the width of one of the grey areas. A smaller well defined penumbra results in less healthy tissue receiving a dose.

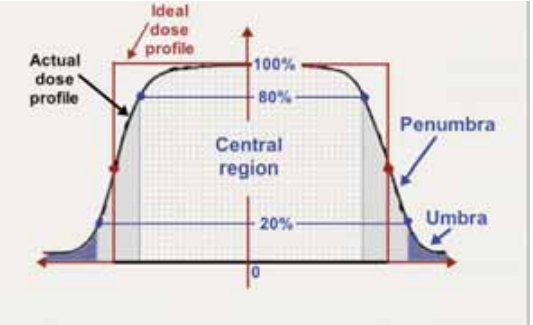

Figure 2.10: lateral distribution of dose profile (black), ideal dose profile (red), penumbra (grey area) and umbra (blue area). Figure from: Podgorsak [35]

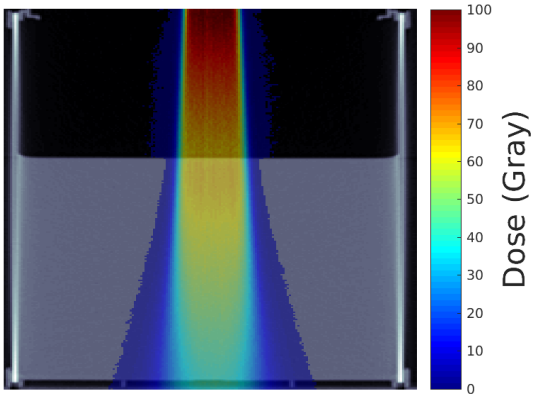

Figure 2.11: CT image of a water tank with an overlay of the simulated dose profile in colour. The tank is partially filled with water. Figure generated for this thesis, with dose calculated using TOPAS MC with 100 MeV electrons.

Scattering events will cause the beam to broaden which means the penumbra will increase. Scattering will occur due to travel in a medium. So we expect the penumbra will increase if a larger distance is travelled. In the previous section we found that the stopping power of electrons decreases with increasing electron energy (up to about 1 GeV).

Figure 2.12 shows the penumbra for electron beams with 1225 pencilbeams in a cartesian grid of 35 x 35 pencil beams with spacing 3 mm. Curves in the figure are calculated for energies between 100 and 900 MeV in steps of 100 MeV. From the figure we can see that the penumbra of the 100 MeV beams reaches 100 mm at a depth of 600 mm, while the higher energy beams keep a smaller penumbra of 25-30 mm. The interaction probability for electrons at higher energy is reduces, resulting in scattering events.

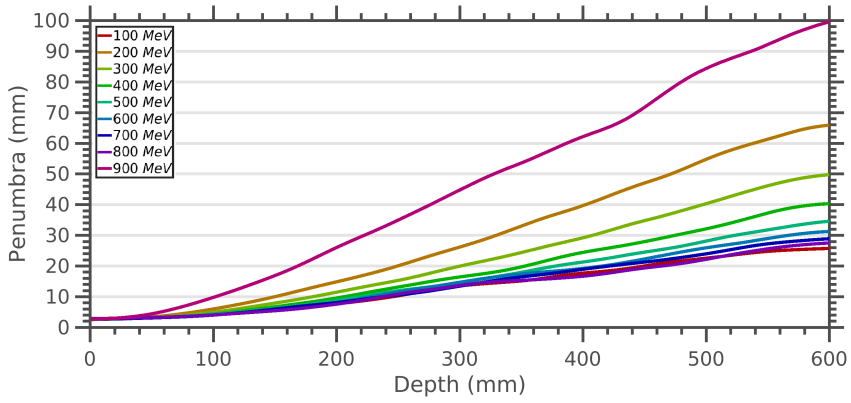

Figure 2.12: Penumbra of full electron beam in water tank. Beam contains 1225 pencil beams in 35x35 grid with 3 mm spacing. Colours range from red (100 MeV) to purple (900 MeV).

2.4.2. Percentage depth dose

The percentage depth dose (PDD) shows the dose over depth. We can use on-axis PDD which shows the dose deposited at a particular depth. Alternative method is the integrated PDD which shows the total dose deposited at a particular depth. In Figures 2.13 and 2.14 the on-axis and integrated depth dose are shown for photons and electrons.

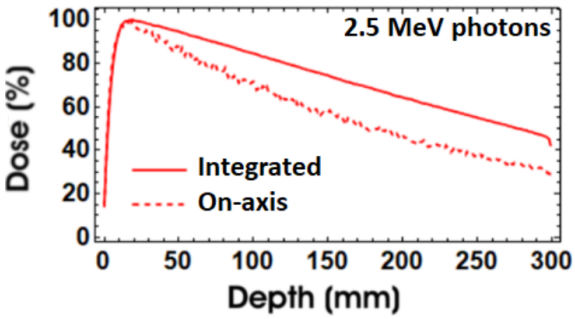

Figure 2.13: Percentage depth dose for photons. integrated PDD (solid) and on-axis(dashed). Figure from: Lagzda [22]

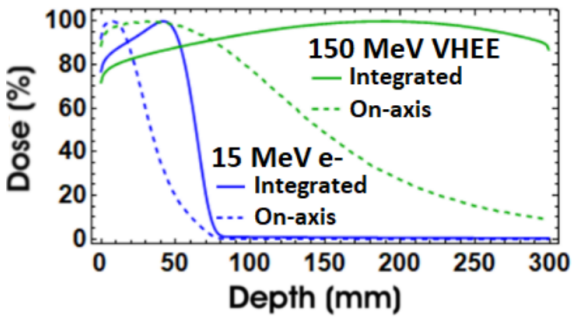

Figure 2.14: Percentage depth dose for electrons of 15 MeV (blue) and 150 MeV (green) for beams with a gaussian beam spread of 5 mm. Integrated PDD(solid) and on-axis(dashed) . Figure from: Lagzda [22]

The difference between integrated and on-axis dose profiles is due to scattering at greater depths which is included in the integrated lines but not the on-axis. In Figures 2.15 and 2.16 we see the on axis and integrated PDD for electrons with energies between 100 and 700 MeV. The peak of maximum energy moves toward greater depth for higher energies. The main effect of higher energies is the increase in dose beyond the maxium dose. This means we should see a higher dose behind a tumor if we use higher energy electrons.

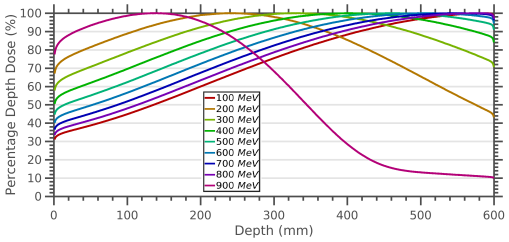

Figure 2.15: Integrated depth dose for 100 to 900 MeV electrons in water. The simulations used 1225 pencil beams in a 10 by 10 cm grid spaced 3 mm.

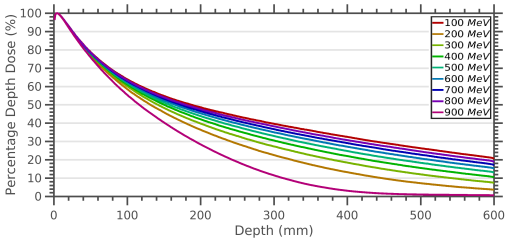

Figure 2.16: On axis percentage depth dose for 100 to 900 MeV electrons in water. The simulations used 1225 pencil beams in a 10 by 10 cm grid spaced 3 mm.

We obtain a well-defined beam if we use high energy electrons but the intensity will be greater on the central axis. Healthy tissue before and after the tumor will receive a higher dose, only the penumbra is smaller, so the high dose area is also smaller.

2.4.3. lateral distribution

In Figures 2.17 and 2.18 the lateral distributions of the electron beam are shown for depths of 10 and 30 cm. lateral distribution are the 1D dose profile perpendicular to the propagation direction. Each of the energy's lateral distribution has been normalized to the maximum of their 3D dose matrix. The lateral distribution broaden with propagation in a medium due to scattering. We see in Figure 2.17 a narrower lateral distribution for greater energies. Figure 2.17 shows that when electrons propagate deeper into matter higher energy electron beams maintain a narrower lateral distribution with a higher peak dose.

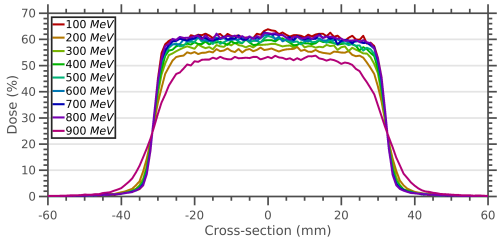

Figure 2.17: Lateral distribution at a depth of 10 cm of the normalized dose for 100 to 900 MeV electrons in water. Normalized to maximum of 3D dose matrix. The simulations used 1225 pencil beams in a 35x35 grid spaced 3 mm.

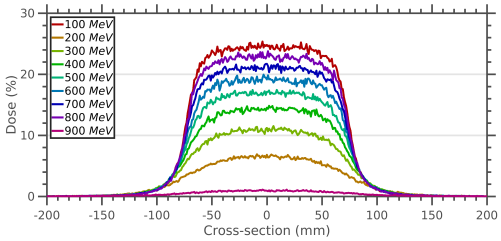

Figure 2.18: Lateral distribution at a depth of 50 cm of the normalized dose for 100 to 900 MeV electrons in water. Normalized to maximum of 3D dose matrix. The simulations used 1225 pencil beams in a 35x35 grid spaced 3 mm.

2.5. Monte Carlo Simulations

In this section we focus on the computational method. This method is used to determine where an electron emitted from the radiotherapy equipment will cause tissue damage. We cannot actually know if damage is caused by a single particle so we will be looking at the absorbed dose. This variable shows how much ionizing radiation has been absorbed by the body with the unit Gray (J/kg) with symbol Gy.

Simulations of treatment plans can be done by Monte Carlo (MC) simulations. These are numeric computations relying on random sampling. This method works great with particle physics due to the inherent stochastic nature of particle interactions. The probability of a particle interaction is based on the size of a cross-section. These cross-sections are particle type, matter and interaction specific.

Algorithm 1: Pseudocode of Monte Carlo simulations

```
Define geometry
Define beam
Define scoring
Number of particles N
while i <= N do
    start History
    Generate initial conditions particle (pseudo) randomly from a probability distribution
    while E > E_min do
        Sample distance traveled
        Transport particle
        Transport particle to interaction site
        Determine interaction type
        Sample exit energy and direction and secondary particles
        Add to history
    end
    Add history to scoring
end
```

The procedure for Monte Carlo simulations is shown Algorithm 1. We first determine the geometry of our world. For radiotherapy we would use a CT image from the patient. The beam needs to be define. This requires a location with density distribution for energy, angle and position. The scoring method should be defined so the system knows what information needs to be saved. The last variable is the number of particles. This needs to be sufficient to gain statistical certainty. The simulations will take longer to run for an increasing number of particles.

For each particle we will save a history. A history contains the steps a particle has taken as well as its energy. Interactions can result in new particles. These are added to the history and tracked as well. The loop stops when all particles have an energy below E_{min}. This energy cut-off is necessary because as the energy drops the number of secondary particles increases exponentially.

2.6. Treatment plan optimization

We expose the patient to radiation from several directions with beams that overlap at the tumor to maximize the tumor dose relative to the healthy tissue surrounding it. This is shown in Figure 2.1. For optimization we need to determine the number of beams and their directions, as well as the 2D fluence distribution of each beam. For this report we focus on pencil beam scanning. So the 2D profile will be a discrete uniformly spaced field of pencil beam positions. The plan optimization is used to determine the optimal distribution of intensity over the pencil beams. Figure 2.19 shows the selection of pencil beams for one beam direction. For pencil beam scanning the tumor is discretized based on the user defined pencil beam spacing. From this we back-propagate to the source. To determine the required pencil beams.

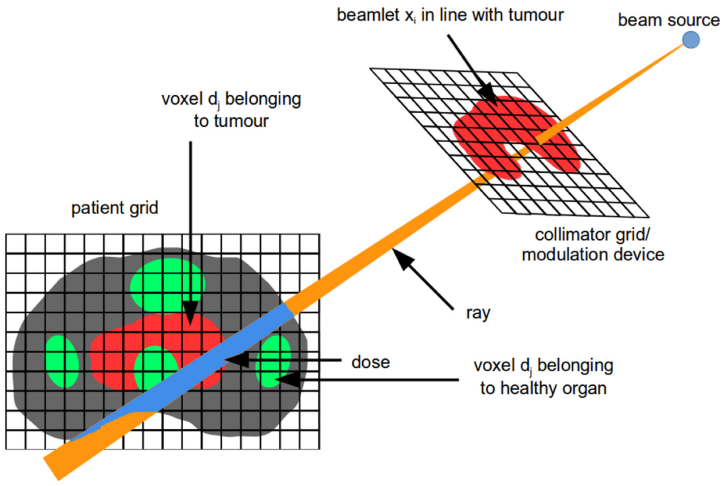

Figure 2.19: Schematic of beamlet selection for radiotherapy. From the source we draw a ray to each voxel belonging to the tumor. The collimator grid shows the location of all the required beamlets to fully cover the tumor. Figure from: Breedveld and Heijmen [6]

Typically optimization of a treatment is performed for a user selected set of beam directions. This is done to achieve a reasonable optimization time. The treatment plan needs to be optimized for each user selected beam angle and the pencil beams within each of these beam angles. The optimization is based on multi-criteria which gives opportunities to generate the highest quality treatment plans.

Each structure (e.g. left femur, spinal cord, tumor) has its specific criteria and as such adds to the complexity of the problem. There are multiple methods of achieving a multi-criteria treatment plan optimization. In this report we will focus on the workings of Erasmus-iCycle [7]. This method uses a user defined wish-list with constraints and objectives.

The algorithm optimizes the dose distribution in the patient in two ways. It determines the dose profile for each beam and in which order the beams are to be optimized.

3

Literature Study VHEE

The first feasibility study on VHEE in relation to radiation therapy was found in DesRosiers et al. [11]. Radiation therapy using electrons in the range of 150 to 250 MeV was researched. The authors used Monte Carlo simulations to evaluate the potential of the electrons for use as a clinical modality in radiation therapy. Simulations were performed with PENELOPE on a homogeneous target medium, with no validation of the model due to inaccessibility of electron beams of this type.

The pencil beam design is mentioned as a critical design component, but the authors have not provided clarification of their design decisions. This should to be researched to assess feasibility of VHEE as a therapy modality.

The results show penetration depths greater than 40 cm, which would be sufficient for clinical applications. A favorable depth dose distribution of electron beams compared to photon beams is found.

Lief et al. [25] suggested magnetic beam scanning could be a potential targeting method. DesRosiers et al. expects the use of beam scanning will be a significant time saving over mechanical multi-leaf collimator. With a similar treatment times VHEE therapy can use more beam angles resulting in superior treatment plans. In Figure 3.1 a schematic of pencil beam scanning is shown. We can scan the target by applying a magnetic field in the path of the electron beam resulting in a deflection. Increasing the field strength will deflect the electron beam more. For use in a clinical setting we will need two magnets so we can scan in a plane. An alternative method would be to use two magnets for each direction, but with the second magnets polarity reversed. The first magnet will deflect the particle and the second magnet results in the same magnitude of deflection but in opposite direction. With this method all beams would be parallel to each other, but with an offset from the propagation axis z.

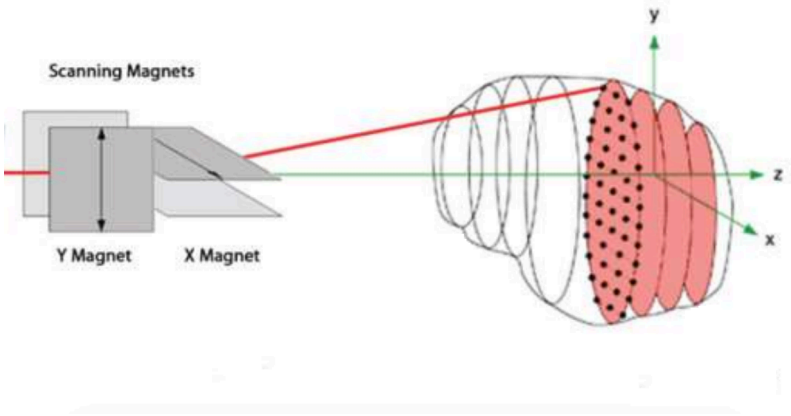

Figure 3.1: Scanning of pencil beam through the use of a set of magnets. Allowing freedom in the x and y direction. Figure from presentation by Depuydt [10]

Evaluation of a VHEE therapy plan was performed by Yeboah et al. [45]. For this evaluation the authors used a simplified prostate cancer model. The pencil beam dose kernels in water were simulated using Monte Carlo Simulations in PENELOPE. To optimize the plan a simple importance model was used to give certain body part higher priority.

The results show that increasing the number of beams improves the target dose distributions and normal tissue saving. Increasing the number of beams beyond $19 - 21$ has shown no benefits to the target dose, but does show an increase in normal tissue dose. The beams were arranged in an equally spaced pattern around the patient in the coronal plane. Rotating the nine beam field arrangement by 10 degrees showed a difference of 20.8% in target dose homogeneity between best and worst plan. This also resulted in an increase of $4 - 6\%$ in integral dose to normal tissue. Selection of beam directions has a considerable impact on plan performance and should be considered in future studies.
The authors found that use of electron with energies greater than 100 MeV results in improved target dose distributions and normal tissue saving. Combining multiple energy beams might lead to improved target dose distributions.

Yeboah and Sandison [44] compared intensity-modulated VHEE therapy, proton therapy (IMPT) and photon therapy (IMRT) plans. The IMPT target dose distribution is superior to VHEE by 1.3% and reduced dose to normal tissue of $17 - 23\%$. While VHEE therapy was found to be comparable to IMRT in target dose distribution, VHEE provided an improved normal tissue saving of 10%. For both of the above mentioned articles it should be noted that no radio-biological effects and inhomogeneities have been taken into account.

Comparison of interface transitions was researched by Papiez et al. [33]. They found VHEE beams showed a uniform dose distribution at the interface between different tissue densities while photon beams resulted in highly inhomogeneous dose distributions.

3.1. Beam characteristics

3.1.1. Experimental

The influence of beam characteristics on the dose distribution should be investigated to determine the potential design parameters of a VHEE treatment setup. In this section the well-documented experimental data on beam characteristics have been summarized in chronological order in Table 3.1. We have included the following categories; Beam type, Detector type, Energy, Divergence, source to surface distance (SSD) and Cross section.

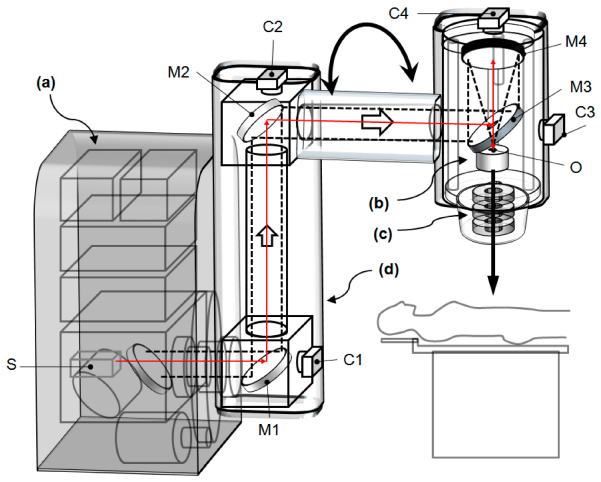

Figure 3.2: Concept of LWFA for use in a clinic setting. The main components are: a) drive laser system, b) Electron accelerator, c) focusing and scanning lenses and d) laser light guidance system. Figure from Nakajima et al. [31]

Beam type refers to either Laser-plasma Wakefield acceleration (LWFA) or Photo-Injector linear accelerator (PI linac) setups. Although there are multiple accelerator designs only LWFA and PI linac setups have been found in literature on VHEE therapy.

LWFA is a method of accelerating electrons. By propagating a laser pulse through a dense plasma, ions and electrons are separated producing a strong electric field. This separation happens due to the creation of wakefields under influence of the laser. The wakefields propagate the electrons but not the heavier ions. Similar to surfing a wave the electrons are accelerated by the plasma wave. The LWFA design is influenced by the plasma itself, the incoming driving laser and the method of injecting electrons into the plasma (either self-injection or using an injection laser). In Figure 3.2 a potential setup for a LWFA therapy machine is shown. It is believed this would fit in a standard therapy bunker. Benefits of LWFA would be short pulse time, high potential energy (quasi-mono energetic) and a small footprint [31]. A LWFA setup that would be suitable for clinical use has yet to be build, so precise beam characteristics are unknown.

A large portion of experimental results are from Photo-Injector linear accelerator. Linear accelerators use an alternating electric potential along a beam line to accelerate the particle. The photo-injector generates an intense beam of electrons, which get accelerated to the required energy levels by the linear accelerator. This setup allows for more flexibility in parameter selection, compared to LWFA. To get energy levels sufficiently high the linear accelerator requires a large footprint making it unsuitable for use in a clinical setting. In Figure 3.3 a typical setup is shown. The PI linac can produce high intensity quasi-mono energetic beams with small cross-sections/divergence. Although PI linacs can not be used in a clinical setting their results can still be used if parameters are comparable to those of a LWFA setup.

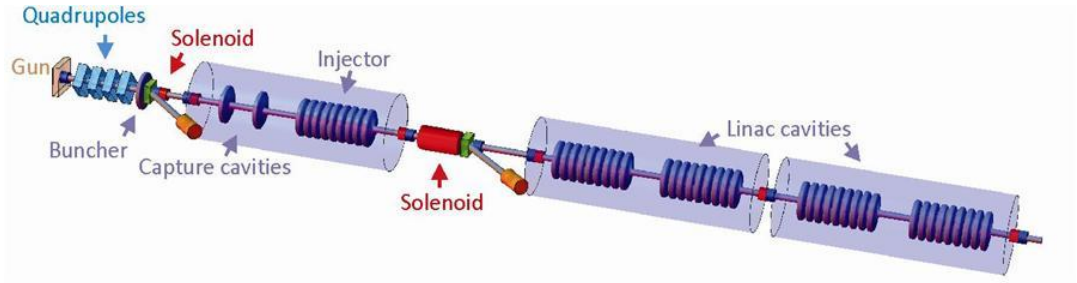

Figure 3.3: Typical Photo-injector Linear accelerator setup. Figure from: Canada's particle accelerator centre

The presented papers detected the electron beams by means of: magnetic spectrometer, radiographic film or a combination of an ion chamber and electrometer. A magnetic spectrometer uses a magnetic driven field to diverge the electrons to a detector screen. The angle under which the electron deflects is correlated to the electrons energy. This method counts the number of electrons in a given energy range. Using a 2D array the electron spectrum is captured in the dispersing plane (see Figure 3.4), while the radial distribution is represented in the transverse plane.

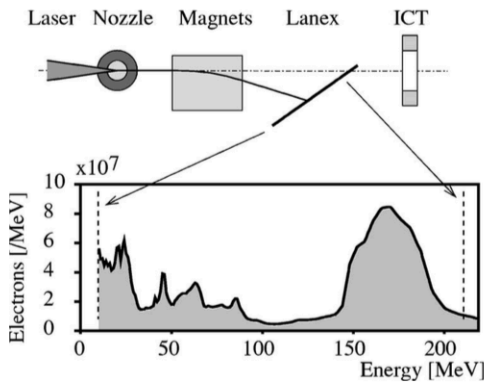

Figure 3.4: Schematic representation of a magnetic spectrometer. Figure from: Glinec et al. [15]

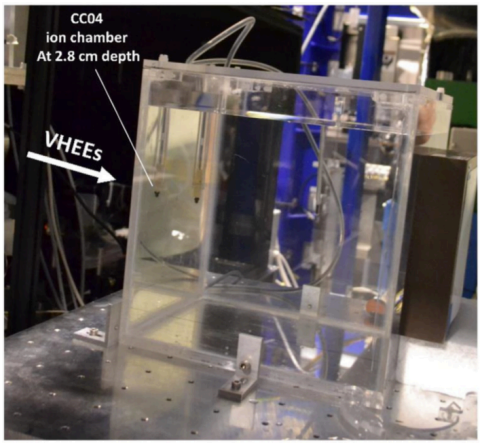

Figure 3.5: Picture of a ion chamber use in a setup. Figure from: Subiel et al. [42]

Radiographic film is photo sensitive paper in a particular energy range. Resulting in both electron and photon detection at a specific depth. Due to the size of the film, multiple can be used to take measurements at different depths. An other method is the use of ion chambers, widely used in clinical settings to validate treatment plans. Typically a small glass vial is used as the ion chamber as can be seen in Figure 3.5. The ionization due to irradiation results in a measurable voltage over the chamber. This in turn can be related back to the dose deposited in the ion chamber. With this method we can take localized measurement in three dimensions in a water tank.

In Table 3.1 the energy reported by the papers is shown, this refers to the beam energy at the exit of the accelerator. If available the Full Width Half Maximum (FWHM) is given. Divergence of the beam is only available for a few articles. In Figure 3.6 this angle is shown as S. Source to surface distance (SSD) is an important variable, for a clinical setting we need at least a SSD of 50 cm. The use of much larger source to surface distances will increase the divergence of the beam. The cross section refers to the plane perpendicular to the propagation axis of the beam (in Figure 3.6 D is half length of the cross section). For all measurements the cross section values are taken at the surface of the phantom or at a shallow depth within the phantom.

Measurement uncertainty have been reported by a few articles:

- Malka et al. [28] found: 5% Peak Energy, 20% Energy spread and 30% divergence at one Standard Deviation (SD),
- Bazalova Carter et al. [3] found an overall uncertainty of 5.5% at one SD.
- Subiel et al. [41] found their dose measurements to be within $3.5 - 5.4\%$ of a SD. All experiments used either a water phantom or polystyrene phantom.

Table 3.1: Reported experimental results of very high energy electron beam characteristics. All measurements were taken using a water phantom. The cross section is defined in the plane perpendicular to the propagation at the beginning of the phantom.

Author (Year)	Beam type	Detector	Energy (FWHM)	Divergence	SSD	Cross section
Glinec et al. [15]	LWFA	Magnetic spec.	$170(40)$ MeV	10 mrad	-	-
Fuchs et al. [13]	LWFA	Magnetic spec.	$170(15)$ MeV	-	-	-
Malka et al. [28]	LWFA	Magnetic spec.	$207(12)$ MeV	4.5 mrad	-	-
Lundh et al. [26]	LWFA	Magnetic spec.	$120(20)$ MeV	2 mrad	-	2.5 x 1.8 mm
Subiel et al. [41]	LWFA	radiographic film	135 MeV	-	185 cm	1.6 cm
	PI linac	radiographic film	165 MeV	-	185 cm	0.8 cm
Bazalova Carter et al. [3]	PI linac	radiographic film	$50 - 70$ MeV	-	15 cm	$1 - 5$ mm
Subiel et al. [42]	PI linac	Ion chamber	$165(0.8)$ MeV	-	41 cm	0.9 cm
Lagzda and Jones [21]	PI linac	radiographic film	$197(0.5)$ MeV	-	40 cm	2.02 mm
Lagzda et al. [23]	PI linac	radiographic film	$156(0.5)$ MeV	-	52 cm	1.2 mm

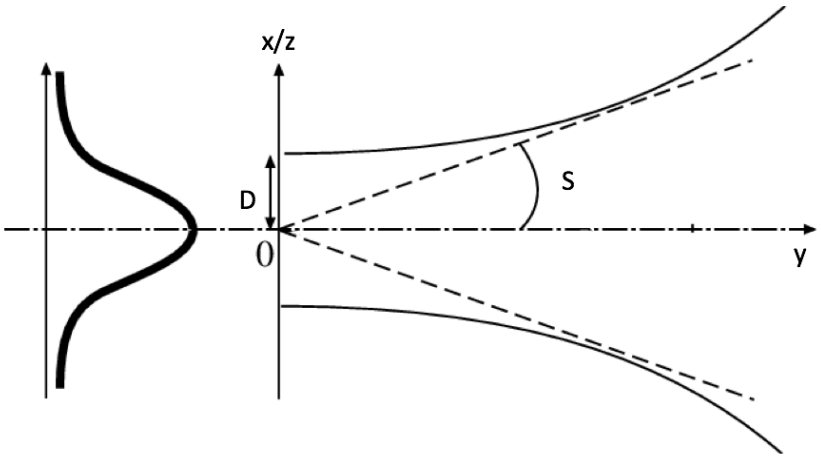

Figure 3.6: Cross-section of Gaussian beam. D is the half length of FWHM for the initial beam. S is the divergence of the beam, x/z the cross-section plane and y the propagation axis Modified version of figure from: Spirou Orchard et al. [40]

Glinec et al. [15] used an magnetic spectrometer, by measuring at multiple positions along the propagation axis determined the electron beam has a nearly constant divergence of 10 mrad at FWHM. Using the same beam type and detector type Lundh et al. [26] showed that the beam is quasi-mono energetic. From all found articles Lundh et al. reported the smallest divergence for a LWFA at 2 mrad. Subiel et al. [41] provided extensive dosimetric data and found the cross section to be quasi-Gaussian at the entrance of the water phantom. This indicates applying a Gaussian approximation in Monte Carlo simulations will be a good fit.

Experimental discussion

The results show a large variation in used setups, with results collected in a 12 years span and limited information on the current advances in LWFA technology. Determining what the potential setup of a VHEE therapy system would be is difficult. We know a quasi-mono energetic beam of up to 200 MeV is possible, with a divergence of as little as 2 mrad. This would mean that for simulation purposes the effects of divergence and energy spread are negligible in comparison tot the effects of electrons scattering in a target. To utilize pencil beams within treatment requires us to maintain a well defined beam spot with a limited penumbra. With the current information the size of the cross section is difficult to predict due to limited information on LWFA setups.

3.1.2. Monte Carlo simulations

Utilizing the findings of experimental studies has allowed for extensive dosimetric evaluation of electron beams. We have chronologically ordered a selection of research on VHEE simulation using Monte Carlo simulations in Table 3.2. MC Software in the table refers to Monte Carlo simulation software. The the majority of articles use Geant4 (GEometry ANd Tracking) Simulation software or a derivative such as TOPAS.

The reported cross section is defined at the surface of the phantom or at a shallow depth within the phantom. The histories value is the number of initial electrons used in the simulation. Kokurewicz et al. [20] mentioned the use of cycles in their article. Cycles are complete runs of the simulation, with a different seeding numbers for the random number generator of the software.

Most of the experiments used a water phantom in their experiments, either with or without a simulated Plexiglas housing. Alternative models include Styrofoam sheets with radiographic film in between.

Fuchs et al. [13] found their experimental results and simulation results for a mono-energetic beam in agreement. In Figure 3.7 a) it is shown that the lateral spread is strongly influenced by the initial beam energy. For an beam energy of 150 MeV the lateral spread is more than 5 cm at a depth of 40 cm, while at the same depth a beam of 250 MeV only has a spread of around 3.6 cm. From Figure 3.7 b) we can see that a large source to surface distance increases the initial beam spread.

Table 3.2: Reported simulation results of very high energy electron beam characteristics. All measurements were taken using a water phantom. The cross section is defined at the entrance of the beam into the water phantom.

Author (Year)	MC software	Energy (FWHM)	Cross section	Divergence	histories (cycles)
Glinec et al. [15]	Geant4	$170(40)$ MeV	-	10 mrad	10^5
Malka et al. [27]	Geant4	$170(40)$ MeV	-	10 mrad	10^5
Fuchs et al. [13]	Geant4	$150 - 250$ MeV $(6.5 - 11.5)\%$	-	6 mrad	$5 \cdot 10^6$
Lundh et al. [26]	Geant4	$110(20)$ MeV	-	-	$7 \cdot 10^7$
Subiel et al. [41]	FLUKA	$165(0.8)$ MeV	4.3 x 3.5 mm	-	10^7
Bazalova Carter et al. [3]	EGSnrc	$50 - 70$ MeV	$1 - 5$ mm	-	10^7
Yoo et al. [46]	Geant4	$113(16) + 120(14)$ MeV	5 mm	20 mrad	$10^5 - 10^7$
Subiel et al. [42]	Geant4	$150(0)$ MeV	-	-	$5 \cdot 10^6$
	FLUKA	$150(0)$ MeV	-	-	10^7
Lagzda and Jones [21]	Geant4	$197(0.5)$ MeV	2.02 mm	-	10^7
Lagzda et al. [23]	TOPAS	$156(0.5)$ MeV	1.2 mm	-	-
Kokurewicz et al. [20]	FLUKA	$200(0)$ MeV + $2(0)$ GeV	Focusing	-	$10^7(5 - 15)$

Bazalova Carter et al. [3] provided extensive comparison between experimental data and Monte Carlo simulations for 50 and 70 MeV. The results showed a close agreement of 4% for the Depth Dose Profile for homogeneous phantoms. The absolute dose difference was shown to vary considerably between 42% and -26%.

Subiel et al. [42] investigated the influence of depth on the energy spectrum. Figure 3.8 a) shows the energy spectrum of electrons at three depths. With propagation of the beam in a medium the maximum energy drops as is expected due to scattering events. The intensity of bremsstrahlung increases with depth for the entire energy spectrum, as can be seen in Figure 3.8 b). Showing for greater depths the main influence on dose will be photon irradiation.

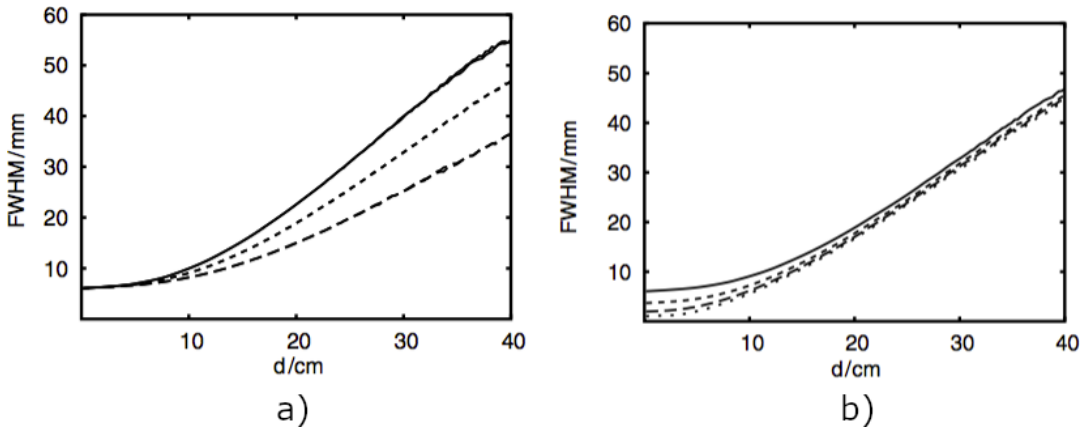

Figure 3.7: a) Lateral spread for 150 MeV (solid line), 185 MeV (short dashed line) and 250 MeV (dashed line). b) Lateral spread for SSD of 100 cm (solid line), 60 cm (short dashed line), 30 cm (dashed line) and 1 cm (dotted line). Figure from: Fuchs et al. [13]

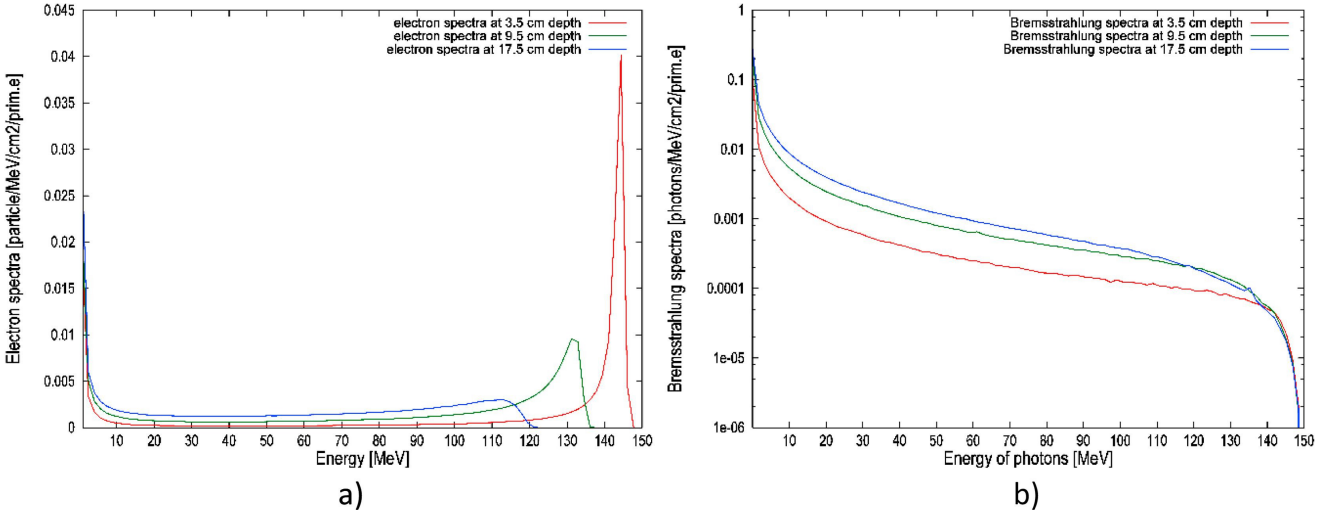

Figure 3.8: a) Shows the energy distribution for depths of (red) 3.5 cm, (green) 9.5 cm and (blue) 17.5 cm. In plot b) the bremsstrahlung spectrum is plotted for the same depths. Figure from: Subiel et al. [42]

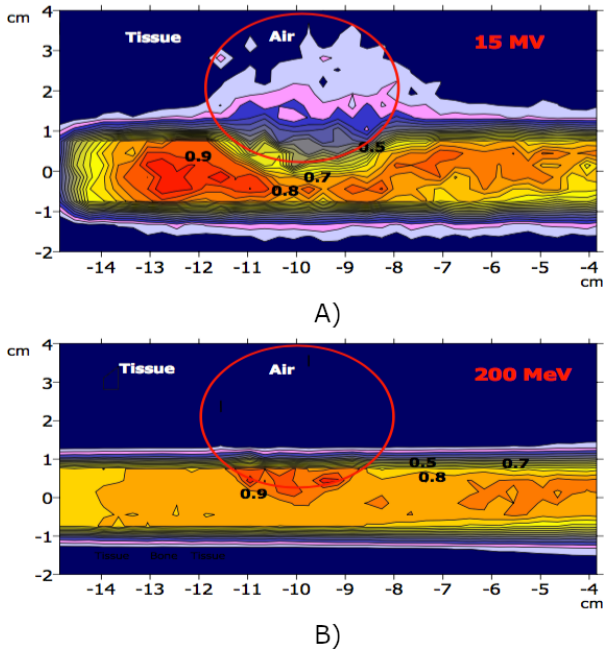

Figure 3.9: Simulation of dose distribution for 15 MV photons (a) and 200 MeV electrons (b). The red circle indicates an air bubble in the tissue. Figure from: DesRosiers et al. [12]

An important question raised by multiple articles is the effect of heterogeneities on the dose deposition and beam behavior. Multiple articles used a spherical tissue model with a small air bubble embedded. The effects of the air bubbles can be seen in Figure 3.9. The 15 MV photon beam is strongly influenced by the air bubble, while for a 200 MeV electron beam no effects are visible.

An approximation to determine the influence heterogeneities were made by Lagzda et al. [23]. They positioned a 2 cm thick insert in the water tank in line with the beam. In Figure 3.10 their results are shown in comparison to a proton beam. The difference between an insert and water is no more than 10% for an electron beam. For proton beams the difference can be more than 50%, although this is more localized. Lagzda and Jones [21] found a maximum deviation of 10% of the depth dose curve for three 2 cm thick inserts (Tufnol,Polypropylene and Teflon), indicating that VHEE can be a potential method of radiotherapy for tumors around the lung or prostate, which are strongly heterogeneous mediums.

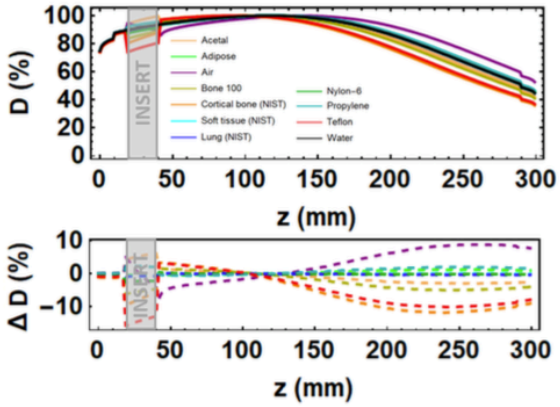

(a) VHEE beams

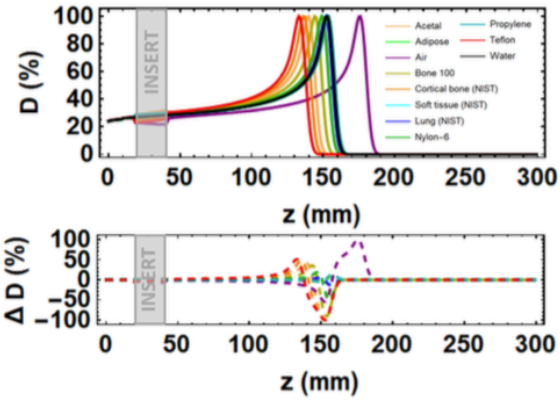

(b) proton beams

Figure 3.10: Depth dose profile and depth dose difference for a) VHEE beam and b) proton beam. Depth dose is given for a selection of materials. The relative depth dose is in relation to water. Figure from: Lagzda and Jones [21]

The review by Malka et al. [28] discussed the potential of LWFA setups with a radiation duration of less than 50 fs to be used for FLASH radiation therapy. FLASH therapy irradiates the patient with a high dose on a femtosecond time scale. This results in little to no normal tissue damage and a high probability of tumor control. It is theorized that this is due to under oxygenation of the tumor, although the workings of FLASH therapy are yet to be understood. This type of therapy has only been tested on animals. [29]

Glinec et al. [15] suggested to use of magnets to focus the VHEE beam. Fuchs et al. [13] investigated focusing with focal lengths of 0 and 30 cm. Building on this research Kokurewicz et al. [20] simulated 200 MeV and 2 GeV beams, while using focal lengths between 1.2 and 11.5 cm. By using a quadrupole magnet the electron beam can be focused with the focal depth as a function of magnetic field strength. In Figure 3.11 the schematic is shown, with focal length being the distance from lens to target. By reducing the magnetic field strength the focal spot size will increase as can be seen in Figure 3.12. Reducing the source to surface distance will move the spot location deeper into the water phantom shown in Figure 3.13.

A problem with VHEE is the lack of skin saving effect and the consequential high entrance dose to the patient. The authors found in their simulations that the peak entrance/exit dose was more than an order of magnitude lower in comparison to an unfocused beam. They were able to create a well-defined focused spot which resulted in an increased dose delivery to the target. At the same time focussing reduced the dose to normal tissue. The authors performed their simulations for 200 MeV and 2 GeV. With the increase in particle energy to 2 GeV a smaller spot size was achieved. For the 200 MeV beam Figure 3.13 a reduction of maximum dose with increasing depth was observed, with a 2 GeV beam on the other hand this pattern is not present.

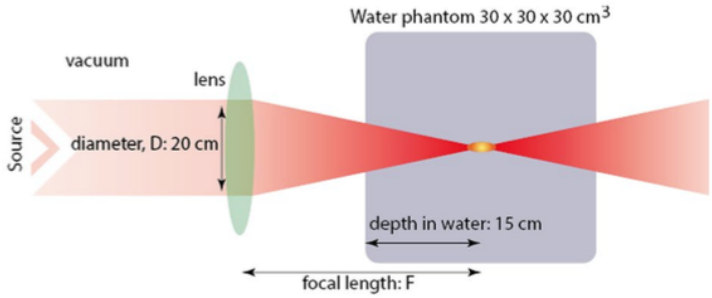

Figure 3.11: Schematic of focusing a VHEE beam. The focusing function represented by a lens will be performed by a quadrupole magnet. Figure from: Kokurewicz et al. [20]

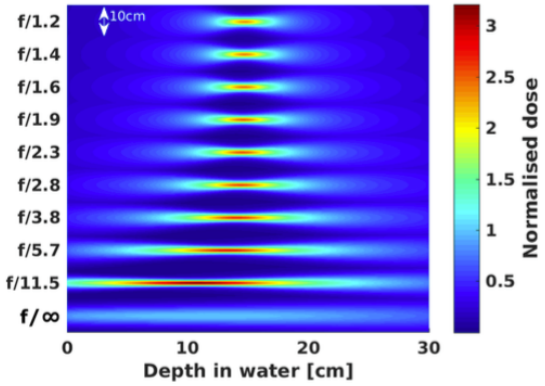

Figure 3.12: Longitudinal 2D cross section of depth dose in water phantom with multiple focal lengths for a 200 MeV beam. Figure from: Kokurewicz et al. [20]

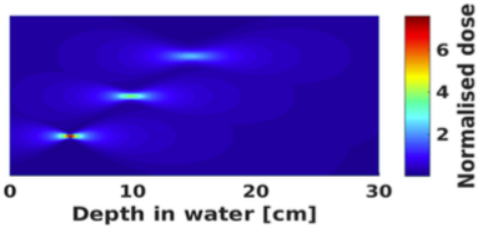

Figure 3.13: Longitudinal 2D cross section of depth dose in water phantom for 5,10 and 15 cm SSD with a 200 MeV beam. Figure from: Kokurewicz et al. [20]

Monte Carlo discussion

All papers which compared their simulation data to experimental results found them to be in agreement. Research up to Subiel et al. in 2014 simplified the beam source to a point source. We found only limited studies concerning inhomogeneities in matter. Research found inhomogeneities showed VHEE to be relatively unaffected. This makes VHEE a promising modality for treatment of lung and prostate cases. The paper by Kokurewicz et al. showed reduction of maximum dose to organs and normal tissue and an improved dose conformity to the tumor by focusing the electron beam. This would be an interesting improvement of VHEE. Focused VHEE might proof to be a cost-efficient alternative to proton therapy, with the capability to approach the proton depth dose profile. Research on FLASH therapy shows great potential although the working principles and long term effects are ill understood.

3.2. Radiotherapy plans

We have found only small number of articles which compared electron therapy with photon and/or proton therapy plans. Multiple articles indicated comparison of treatment modalities is difficult due to lack of dosimetric information on VHEE.

Radiotherapy treatment plans using Monte Carlo simulations, work flow starts typically with selecting the desired beam angles. Followed by calculating the required pencil beams and running the Monte Carlo simulations for all pencil beams individually. After the simulations the optimization algorithm is used to determine the intensity of each pencil beam resulting in a optimized dose distribution. Most research on this topic has been performed by the department of radiation oncology from Stanford University. This group uses RayStation (RaySearch Laboratories AB, Stockholm, Sweden) a commercially available optimization software program, Garnica-Garza [14] used an in house developed optimization program.

Comparison between treatment plans can be made using a variety of methods. Some of these methods such as Homogeneity index (HI) use a formula wich can be defined in multiple ways, we follow the articles definition. We found the following methods

- Dose difference maps, a 2D plot of the dose difference between two variables or modalities.
- Dose-volume histograms (DVH), a graph plot with percentage of volume receiving a certain dose (for example 100% of the body receives 0% dose)
- Minimum/Mean/Maximum dose
- Conformity Indices CI_{50} and CI_{100}, percentage of PTV receiving 50% or 100% of prescripted dose, see Equation (3.1).
- Homogeneity Index HI is an indication of how homogenius the dose distribution to the target volume is using Equation (3.2)

$$CI_x = \frac{V_x}{V_{PTV}} \tag{3.1}$$

with V_x the volume encompassed by x% of the prescription dose and V_{PTV} the volume of the PTV.

$$HI = \frac{D_2 - D_{98}}{D_{50}} \tag{3.2}$$

D_x refers to minimum dose for $x\%$ of the target volume.

A comparison between 6 MV photons and electrons was made by Malka et al. [27]. They found an improved tissue sparing of up to 19% in a clinical prostate case, using a water phantom for the electron simulation data. Fuchs et al. [13] compared intensity modulated VHEE and a 6 MV IMRT treatment plan for a clinical prostate case. The authors approximated the electron pencil beams by assuming a Gaussian lateral distribution, with an integral depth dose as central value. An iterative gradient algorithm optimized the pencil beam weights. The pencil beams spacing was 2.5 mm. The authors reported an increased dose of $1-2$ Gy to the left femur, believed to be due to increased scattering at greater depths. This can be avoided by changing the beam orientations. The use of higher energy electron improved normal tissue saving. Interestingly focusing the beam reduced the mean dose but increased the maximum dose to organs at risk (OAR) and normal tissue. The authors have not used any dosimetric measurements to validate their findings.

Bazalova et al. [2] researched the effect of using a large number of beams (13, 17 and 36) and varying spot size on VHEE treatment plans, with inverse treatment planning. Three cases were reviewed a tumor around the brain stem in a pediatric patient, lung case and a prostate case. The authors compared VHEE to a clinical VMAT 6 MV treatment plan. Increasing the beam energy and increasing the number of beams resulted in a decreased dose in OAR. For the best VHEE therapy plan the mean dose to OAR was up to 70% (temporal lobes 30%) lower in the pediatric case for VHEE. The lung case showed reduced dose as well although to a lesser extent ($19\%-27\%$), no improvement was found in using VHEE in the prostate case. Garnica-Garza [14] found similar results in their study for the prostate case. Further research by Palma et al. [32] build on the research by Bazalova et al. [2]. By using an improved beam design, they showed VHEE therapy to be similar or superior to VMAT for multiple tumor types/locations.

A broader comparison between VHEE, VMAT and Proton Pencil Beam Scanning (PPBS) was performed by Schüler et al. [39] for a lung, pediatric brain, HNC and prostate case. In Figure 3.14 the treatment plan comparison for the lung case is shown. We can see that all modalities deliver the same dose to the target volume, with similar HI and CI values. From the DVH we can see PPBS results in a greatly reduced normal tissue dose, the same is in a lesser extent true for VHEE. PPBS was superior for all cases to both VMAT and VHEE, VHEE showed reduced doses to OAR and normal tissue doses compared to VMAT for lung, pediatric brain and HNC (22%, 75%, and 75%). The authors found a plan with 17 beams to be optimal for VHEE therapy.

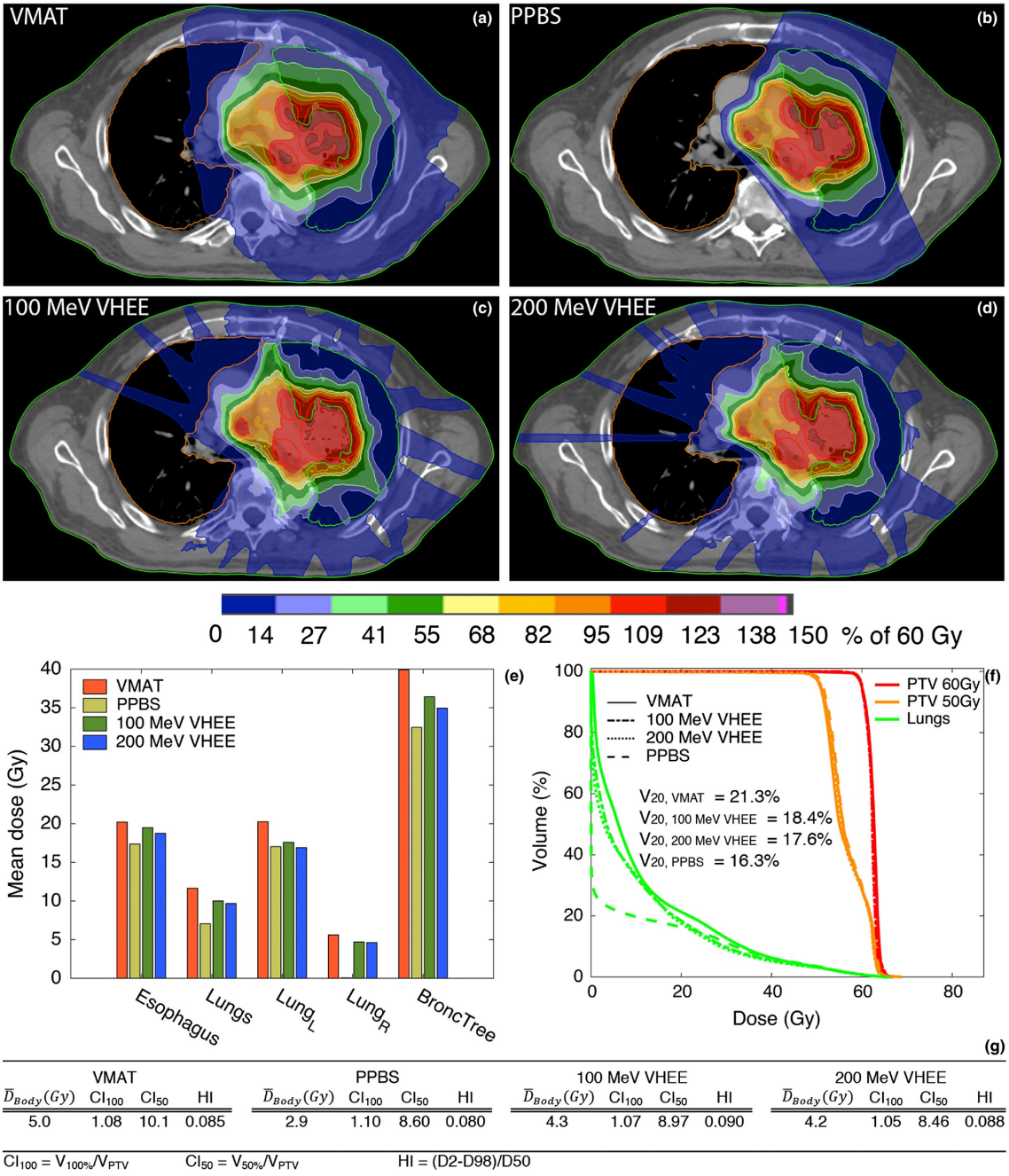

VMAT				PPBS				100 MeV VHEE				200 MeV VHEE			
$\overline{D}_{Body}(Gy)$	CI_{100}	CI_{50}	HI	$\overline{D}_{Body}(Gy)$	CI_{100}	CI_{50}	HI	$\overline{D}_{Body}(Gy)$	CI_{100}	CI_{50}	HI	$\overline{D}_{Body}(Gy)$	CI_{100}	CI_{50}	HI
5.0	1.08	10.1	0.085	2.9	1.10	8.60	0.080	4.3	1.07	8.97	0.090	4.2	1.05	8.46	0.088

$CI_{100} = V_{100\%}/V_{PTV}$ $CI_{50} = V_{50\%}/V_{PTV}$ HI = (D2-D98)/D50

Figure 3.14: Comparison of VMAT, PPBS and VHEE treatment plans for the lung case with (a-d) transverse plane dose distribution. (e) mean dose to selected organs, (f) the DVH and (g) Mean integral dose, CI values and HI. Figure from: Schüler et al. [39]

Treatment plans discussion

Overall studies found VHEE therapy to be at least comparable to IMRT or VMAT and showed proton therapy is in most cases superior in organ/normal tissue saving and dose conformity. Earlier research considerably simplified the problem by not using CT data but a model of humans with only a handful of possible values. Additionally these articles used Monte Carlo simulations to only simulate one pencil beam. Later studies improved on this with actual CT data and full Monte Carlo simulations. Research of actual patients was limited to a few case studies, no large scale studies were performed.

Bazalova et al. found no significant benefits to using VHEE for patients with prostate cancer, but more inhomogenieus treatment locations such as the lungs and brain stem showed potential.

3.3. Conclusion literature study

Research showed VHEE therapy has the potential to be used in clinical setting for treatment of deep seated tumors. The main advantage of VHEE is the relative sharp penumbra at shallow depths and the reduced drop of the depth dose curve, when compared to photons. This results in reduced dose to normal tissue.

Magnetic scanning instead of mechanical scanning reduces treatment time. This allows us to irradiate the patient from a large number of angles for a similar treatment time to mechanical scanning, improving the normal tissue and organ savings. Inhomogeneities in tissue have little effect on Electrons.

Focusing the VHEE beam has potential to be a cost-efficient alternative to proton therapy. For focused VHEE therapy to become a viable alternative more research is needed. The response to inhomogeneities is not well understood and the dosimetric quantities of focusing a VHEE have yet to be experimentally tested. Beside focusing an other interesting new method of dose delivery could be FLASH VHEE.

Only a limited number of treatment plans have been developed, with varying optimization methods making direct comparison difficult. Additionally the ultimate limitation of LWFA are not yet well defined making assessment of beam characteristics difficult.

4

Materials and Methods

This chapter describes the methods used for simulations of the electron beams and the optimization of the treatment plans. First the patient data will be described followed by the workflow and the preparations required for the Monte Carlo dose calculations. After this the optimization steps are listed and finally the tools, used to compare Very High Energy Electrons (VHEE) treatment plans to photon treatment plans, are described.

4.1. Patients

CT images of 10 patients with prostate cancer were included. The 23 beam Intensity Modulated Radiotherapy (IMRT) treatment plans were compared with VHEE treatment plans. Nine of the ten patients had a single Planning Target Volume (PTV). One patient had a more complex tumor layout with 2 PTV zones. For this patient the main PTV was selected to ensure all patients had a comparable PTV. The patient related information was anonymized prior to conducting the research.

4.2. Workflow

VHEE treatment plans were generated using Monte Carlo pencil beam simulations and automated plan optimization. A workflow chart with the steps can be found in Appendix A. The workflow is split into three sections: initialization, Monte Carlo simulations and optimization.

Initialization

From the patient data the PTV location, isocentre and offsets of the CT were importated into MATLAB (version R2017a, The Mathworks, Natick, MA). The user selected beam angles and beam parameters were also imported into MATLAB. Irradiation of the target was performed using pencil beam scanning, for this the location of each pencil beam needed to be determined. Spacing between pencil beams of 3 mm in x and y direction on a cartesian grid was found to be sufficent for obtaining a smooth dose profile with a ripple of less than 1%.

To determine the pencil beam locations within the patient the PTV was project in the direction of the selected beam angle. A cartesian grid, with 3 mm spacing between spots, was overlayed on this projection. The grid was placed at the isocentre of the PTV, the isocentre is defined as the point in space around which the gantry head rotates. Each pencil beam is backpropagated to the source, from which the x and y angle are determined. For this project it was decided that the source-axis distance (SAD), the distance between isocentre and exit window of the source, is constant for all beam angles at 500 mm. The CT images, isocentre position, offsets and the pencil beam angles were saved to a matlab MAT file.

Monte Carlo simulations

Using a python script TOPAS MC (Version 3.2.1, TOPAS MC Inc.) parameter files were generated and saved in txt format to disk, examples of the parameter files are shown in Appendix D and table 4.1. TOPAS MC simulations were executed using the TOPAS parameter files resulting in DICOM dose files

for each pencil beam. The pencilbeam DICOM files were combined into a sparse matlab matrix for each beam angle.

Optimization
Optimizations of the treatment plans were performed by using Erasmus-iCycle treatment plan optimization [7]. Patient data was loaded from the MAT files and extracted from the topas parameter files. This data was used to setup the beam positions, CT data and structure data in Erasmus-iCycle. For each optimization the beam energy and beam angle needed to be selected manually. The wishlist and defined structures used for the optimizations are shown in Appendix B.

4.3. Monte Carlo dose calculations

The Monte Carlo simulations required CT images, isocentre of the PTV and the delineation of all relevant structures. Delineation of a structure is the outline around the volume in 3D. The structure delineations have been performed by the Erasmus MC for all ten patients.

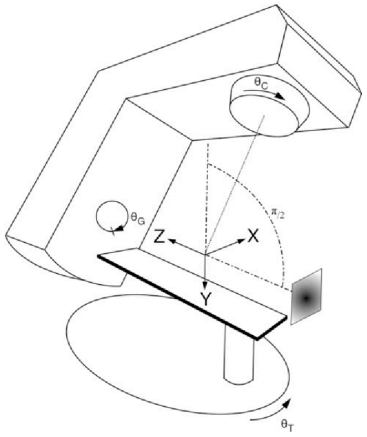

Figure 4.1: The International Electrotechnical Commission (IEC) defined accelerator coordinate system. Figure from: Bush and Zavgorodni [8]

The beam angles were manually selected before the simulations. An equispaced 36 beam layout starting at 0 degrees was used, as defined in Figure 4.1. For each beam the pencil beam angles in x and y direction were determined, as shown in Figure 2.19 in Chapter 2. Generation of the TOPAS parameter files was performed using a MATLAB script. For the parameter files generation the pencil beam grid data; electron beam energy; CT images and isocentre were used. The TOPAS parameter files were generated for each beam angle, an example is shown in Appendix D.

4.3.1. Pencil beam generation

Design of the pencil beam is based on experimental data [3, 13, 15, 22, 23, 26, 28, 41, 42] and has been the focus of the literature study in Chapter 3. The key parameters of the pencil beam used for this project are shown in Table 4.1 and the complete pencil beam parameter file is shown in Appendix C.

Table 4.1: Pencil beam parameters for TOPAS MC.

Variable	Value	Unit
Energy spread	0.5	%
Energy	200,300,400	MeV
Position Distribution	Gaussian	
σ_x	10	mm
σ_y	10	mm
Angular Distribution	Gaussian	
σ_x	3	mrad
σ_y	3	mrad

Before the simulations started both the number of particles used in the simulation and the spread between pencil beams have been studied. The 2D cross-section of a 10 x 10 mm grid of pencil beams has been studied for multiple pencil beam distances. The pencil beam distances being the distance between pencil beams in the x and y direction. Figure 4.3 shows the dose profile for 1-4 mm pencil beam distances at multiple depths (with 10^4 particles). A distance of 3 mm between pencil beams results in a ribble in the dose of less than 1 %. The number of particles used per pencil beam needs to be high enough to achieve an acceptable signal to noise ratio and low enough to achieve acceptable simulation times. Figure 4.2 shows that pencil beams with 10^4 particles result in a close approximation of a gaussian curve, which is expected for the pencil beams. Prelimenary studies showed that using a combination of 10^4 particle per pencil beam with a distance between pencil beams of 3 mm results in a smooth dose profile required for radiotherapy.

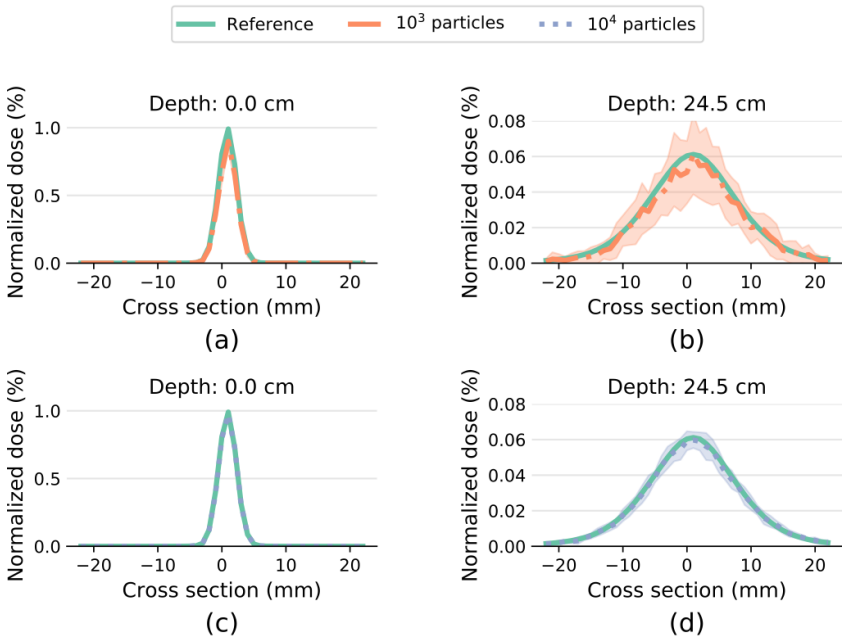

Figure 4.2: Plots show the Normalized 1D cross-section of a pencil beam (n=15), with reference gaussian curve(green), simulation with 10^3 particles (red) and 10^4 simulated particles (dotted blue). plots (a,c) show the cross-section at a depth of 0 mm, and (b,d) show the cross-section at a depth of 245 mm.

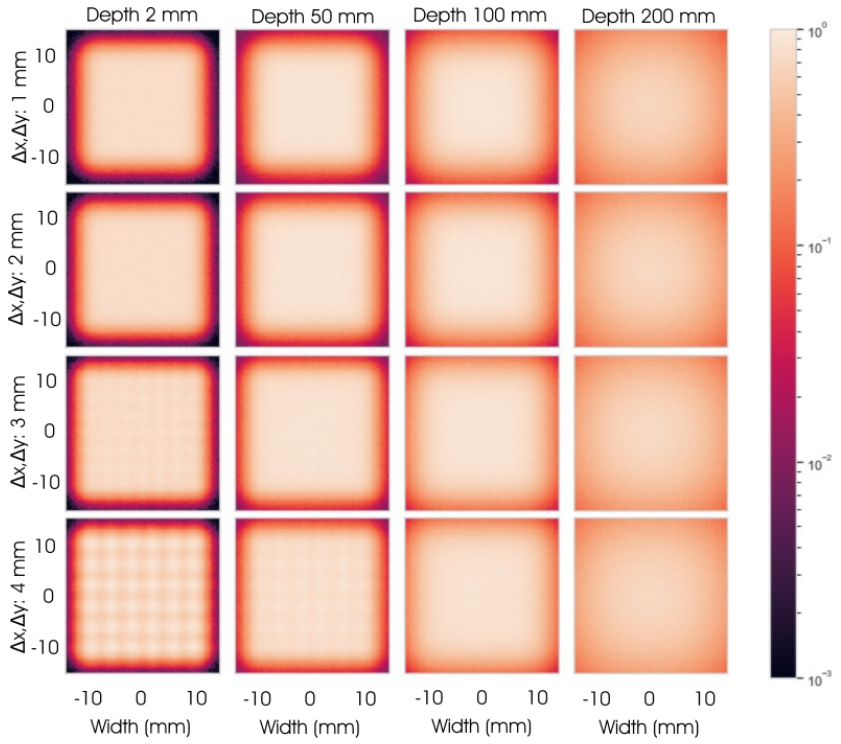

Figure 4.3: TOPAS MC simulation of electron beam dose 2D cross-sections in a watertank. Graphs show the logirithmic dose distribution for cartesian pencil beam grids with 10^4 simulated particles per pencilbeam. Horizontal rows show the different pencil beam distances in x and y: 1 mm, 2mm, 3mm and 4mm. The collums show the depth from entry in watertank.

The literature study showed that among authors the definition of beam specifications for both experimental data and Monte Carlo simulations varied widely. The pencil beam design used for this project follows the design specifications of Subiel et al. [41, 42] as closely as possible. The authors researched both experimental setups and Monte Carlo simulations for VHEE. The experimental studies by Subiel were performed on a Laser Wake Field Acceleration (LWFA) and linear accelerator (linac). For this project the used beam parameters were within the range found in the literature study. The positional and angular distributions needed to be calculated based on the provided cross-section and SAD information.

4.3.2. TOPAS MC output

TOPAS MC provides a 3D dose dicom file for each pencil beam in a beam angle simulation. This means that a large number of files per beam angle were generated. The 3D dose files were converted to sparse vectors removing only zero valued voxels. The vectors were combined into a 2D sparse matrix and saved as matlab MAT files.

The sparse data was stored to disk resulting in approximately 1-2 GB of data per beam angle depending on CT image size, number of pencil beams and their angle. This data was used to perform the Erasmus-iCycle optimization.

4.4. Optimization of treatment plans

Pencil beam dose data from TOPAS MC were imported into Erasmus-iCycle and prepared for optimization. For the optimization a wishlist needed to be prepared. The wishlist was developed with the help of Abdul Wahab M. Sharfo (Department of Radiation Oncology, Erasmus MC Cancer Institute, Rotterdam).

4.4.1. Plan generation

The treatment plans were generated for electron beam energies of 200, 300 and 400 MeV. All the generated treatment plans are shown in Table 4.2. For all patients, both 18 and 36 beam treatment plans were generated using all three electron beam energies. Furthermore treatment plans were simulated for 200 and 300 MeV with 9 beams. In total 7 treatment plans were generated for each patient. For 6 patients treatment plans were simulated using two beam energies: 18 beams of 200 MeV and an overlapping 18 beams of 300 MeV into a 36 beam plan. The treatment plans were generated for a target PTV dose of 60 Gy.

Table 4.2: Generated VHEE Treatment plan.

Energy (MeV)	Beams	Patients
200	9,18,36	2, 6, 9, 10, 16, 18, 22, 24, 29, 30
300	9,18,36	2, 6, 9, 10, 16, 18, 22, 24, 29, 30
400	18,36	2, 6, 9, 10, 16, 18, 22, 24, 29, 30
200 + 300	36	6, 10, 16, 18, 22, 24

The wishlist used for the optimizations can be found in Appendix B. Figure B.1 in the appendix shows the constraints and objectives. The wishlist used for optimization of the treatment plans contains multiple constraints and objectives for the PTV and some Organs at Risk (OAR).

The objectives were optimized by minimizing either the mean, (Logarithmic Tumor Control Probability) LTCP, linear maximum/minimum dose or Equivalent uniform dose (EUD) of the structure. The LTCP cost function was used for the PTV, which is described by the expression from Alber and Reemtsen [1]:

$$LTCP = \frac{1}{m}\sum_{j=1}^{m} e^{-\alpha(d_j - D^p)} \tag{4.1}$$

With m the number of voxels in the structure, D^p prescribed dose, d_j dose in voxel j and α the cell sensitivity. The LTCP minimization was used to obtain a smooth dose profile in the PTV. The design of the wishlist was centered around the PTV, where a smooth dose profile needs to be obtained while maintaining a sharp dose drop off at the edge of PTV. Rings around the PTV were created, with the objective to stepwise reduce the dose. The rings around the PTV are shown in the figure of Appendix B.

The wishlist is identical for all treatment plan optimizations. Due to the problem size and calculations time, voxel sampling had to be reduced for the 36 beam plans from 300 to 200 voxels/cc in the PTV structure and from 50 to 20 voxels/cc for the external ring.

4.4.2. Automated generation 23-beam IMRT plans

To make the comparison between the IMRT and VHEE treatment plans both were optimized using Erasmus-iCycle. The IMRT wishlist had the same constraints and objectives, but used shells around the PTV instead of the volumetric rings of the VHEE wishlist.

Clinical IMRT plans contain a beam delivery correction in the form of a collimator segmentation correction. These corrections were not used in this project, because currently no information on the beam delivery corrections of VHEE beams exist.

4.4.3. Plan quality evaluations

A number of methods was used to quantify the difference in treatment plan quality. The treatment plans were compared using the dose profile maps, Dose Volume Histogram (DVH), Conformity Index (CI), mean dose and Volume dose metrics.

Three conformity indices CI_{95} CI_{50} and CI_{riet} were calculated to compare the treatment plans. CI is the ratio between volume covered by the reference dose and the target volume. Conformity index CI_x was calculated with

$$CI_x = \frac{V_x}{V_{PTV}} \tag{4.2}$$

Here V_x is the volume of all voxels inside of the PTV with a dose of $x\%$ of the prescribed dose. V_{PTV} is the PTV volume. CI_{riet} uses the following formula

$$CI = \frac{TV_{RI}}{TV} \cdot \frac{TV_{RI}}{V_{RI}} \tag{4.3}$$

Here TV is the volume of all voxels inside of the PTV. TV_{RI} is the volume within the target covered by the prescription dose. V_{RI} is the volume of the prescription dose.

An other method of assessment of treatment plans used in this project is the percentage of a volume that has a dose of at least x Gy. For this metrics we use the symbol V_{xGy}. Maximum dose is an other metrics to assess the quality of the treatment plan, for this the $D_{0.001cc}$ was used. This metric shows the maximum dose that is found in at least 0.001 cc of a volume.

The dosimetric parameters are presented as the mean ± 1 standard deviation. T-tests were performed to determine the significance of differences in parameter values. Paired two-sided Wilcoxon tests were performed to determine the significance of the observed differences, because the parameter values were not sufficiently resembling a normal distribution. A p value < 0.05 was considered statistically significant [43].

5

Results

This chapter will discuss the population average IMRT treatment plan compared with the population average VHEE treatment plans. Section 5.1 compares the IMRT treatment plan with 300 MeV VHEE treatment plans using 9, 18 and 36 beam. Section 5.2 compares IMRT with 18 beam VHEE treatment plans using 200, 300 and 400 MeV. Section 5.3 evaluates the effect of combining multiple energies in a single treatment plan and the last section shows the performance metrics of the Monte Carlo simulations and treatment plan optimizations.

5.1. Comparing treatment plans with 9, 18 and 36 beams

The IMRT plan is compared with the VHEE treatment plans for 9, 18 and 36 beams. The axial dose distribution and dosimetric parameters are presented for the VHEE treatment plans with 300 MeV and the DVHs are shown for all electron beam energies.

As an example the axial dose distributions for patient 6 are shown in Figure 5.1. The IMRT plan has a smooth dose distribution with broad low dose area's outside of the PTV. The VHEE plans have a dose profile with sharp lines extending from the PTV.

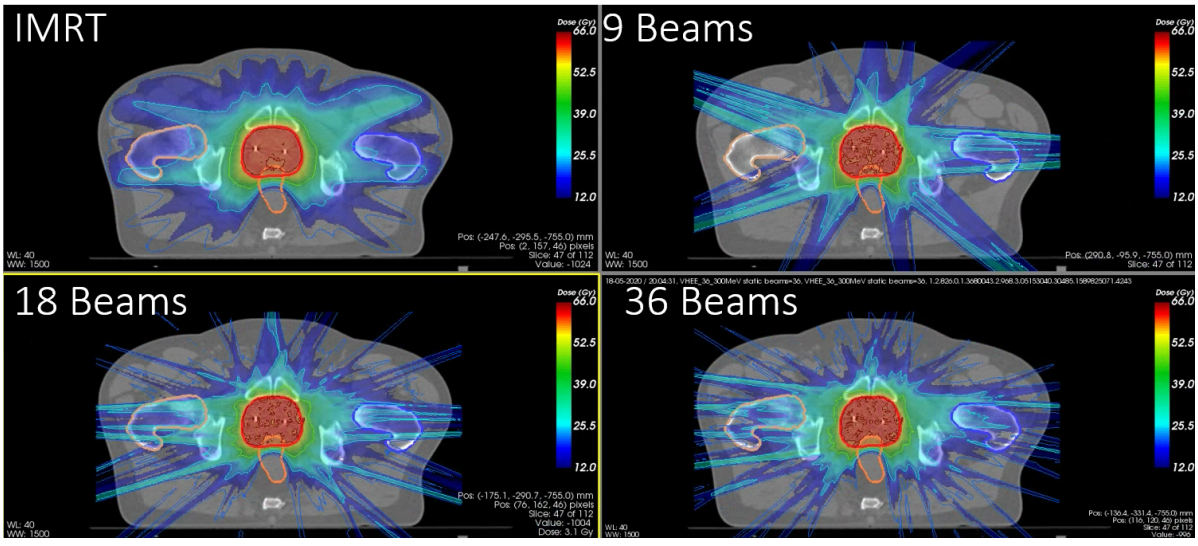

Figure 5.1: Axial dose distribution for Patient 6. Comparing IMRT with 9, 18 and 36 equiangular spaced 300 MeV electron beams.

Figure 5.2 shows the 200 MeV VHEE treatment plan population average DVHs (n=10) for PTV, bladder, anus and rectum. The graphs compare the IMRT plan with the VHEE plans for 9, 18 and 36 beams. The PTV is normalized to a dose of 60 Gy for all plans with a 99 % V_{57Gy} coverage.

The bladder population average DVH is similar for all four treatment plans in the range of 55-61 Gy. In the medium and low dose range the VHEE treatment plans with 18 and 36 beams show considerable reduction in dose, while the 9 beam treatment plan is similar to the IMRT treatment plan.

The rectum DVH of the IMRT plan and the 18 beam plan is similar, while the 9 beam VHEE plan shows higher doses and the 36 beam VHEE plan shows lower doses.

The anus DVH shows that the IMRT plan and the 18 beam VHEE plan result in similar graphs in the medium and high doses range, but the 18 beam VHEE plan reduces the dose volume of lower dose levels. The 9 beam VHEE plan results in higher doses and the 36 beam in lower doses when compared to IMRT.

The dose to the OAR is lower in the 36 beam plan compared to the 18 beam plan and the 18 beam plan dose to the OAR is lower compared to the 9 beam plan.

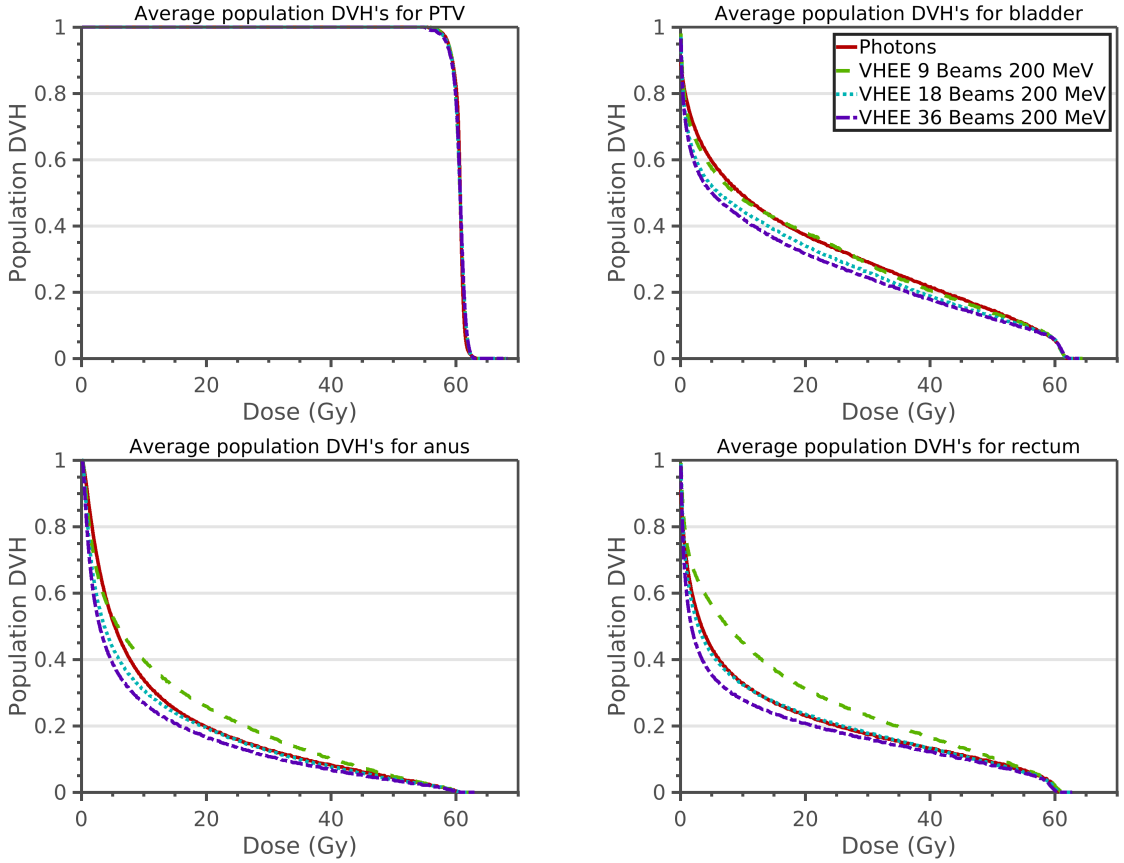

Figure 5.2: Comparisons of population-averaged (n=10) dose volume histograms between IMRT treatment plan and the 9-18-36 beam 200 MeV treatment plans. Graph of the PTV (red), bladder (light blue), anus (dark blue) and rectum (green).

The population average DVHs for 300 MeV electron beam energy are shown in Figure 5.3. The DVHs per patient are shown in the Appendix E Figure E.1 for the patient, femoral head right/left, bladder, anus, rectum and PTV.

All the VHEE treatment plans shows a reduction in bladder dose when compared to the IMRT plan. The 36 beam VHEE plan reduces the bladder dose the most and the 9 beam VHEE plan reduces the bladder dose the least. The anus dose is also reduced by all the VHEE treatment plans. The rectum DVH shows a reduction in dose for the 18 and 36 beam plan compared to the IMRT plan.

The DVHs for the 18 and 36 beam VHEE treatment plan with 400 MeV are shown in Figures 5.3 and 5.4. Both the 18 and 36 beam plan result in considerable reductions in dose to all the OAR. The 36 beam treatment plan results in lower dose to the OAR compared to the 18 beam treatment plan.

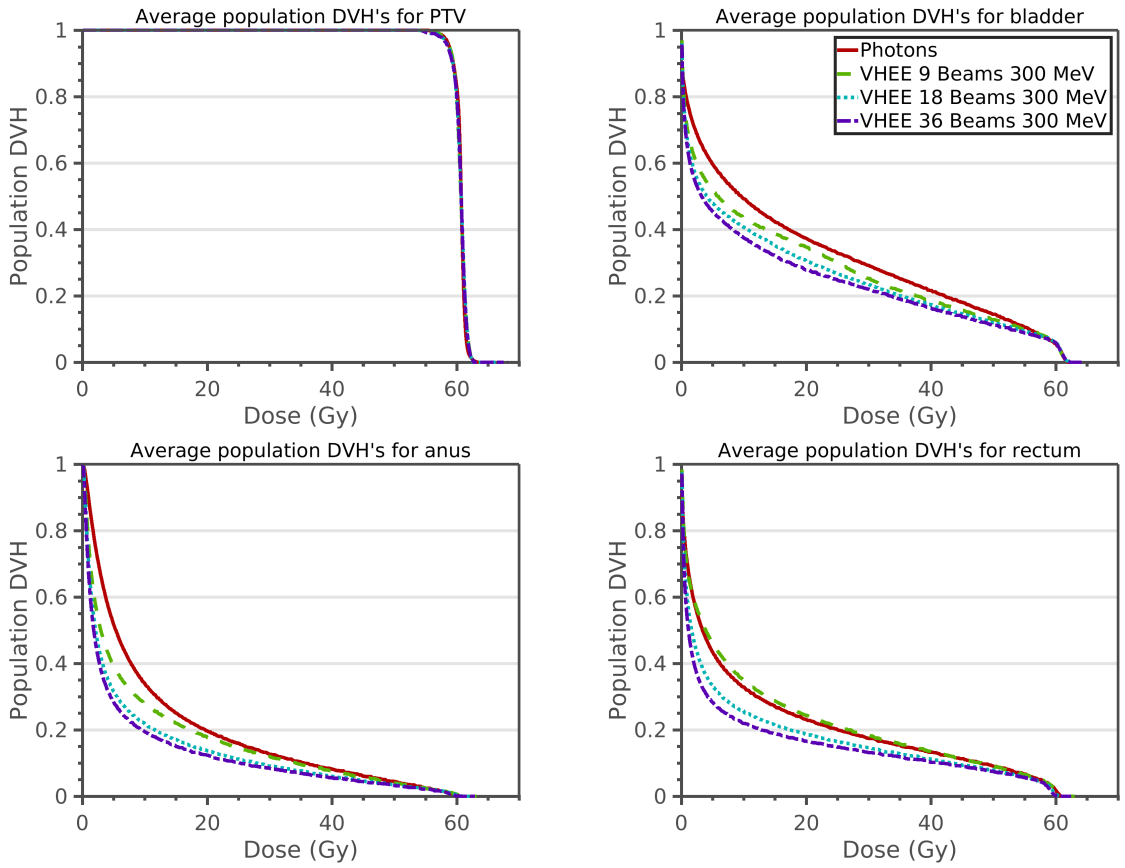

Figure 5.3: Comparisons of population-averaged (n=10) dose volume histograms between IMRT treatment plan and the 9-18-36 beam 300 MeV treatment plans. Graphs of the PTV (red), bladder (light blue), anus (dark blue) and rectum (green).

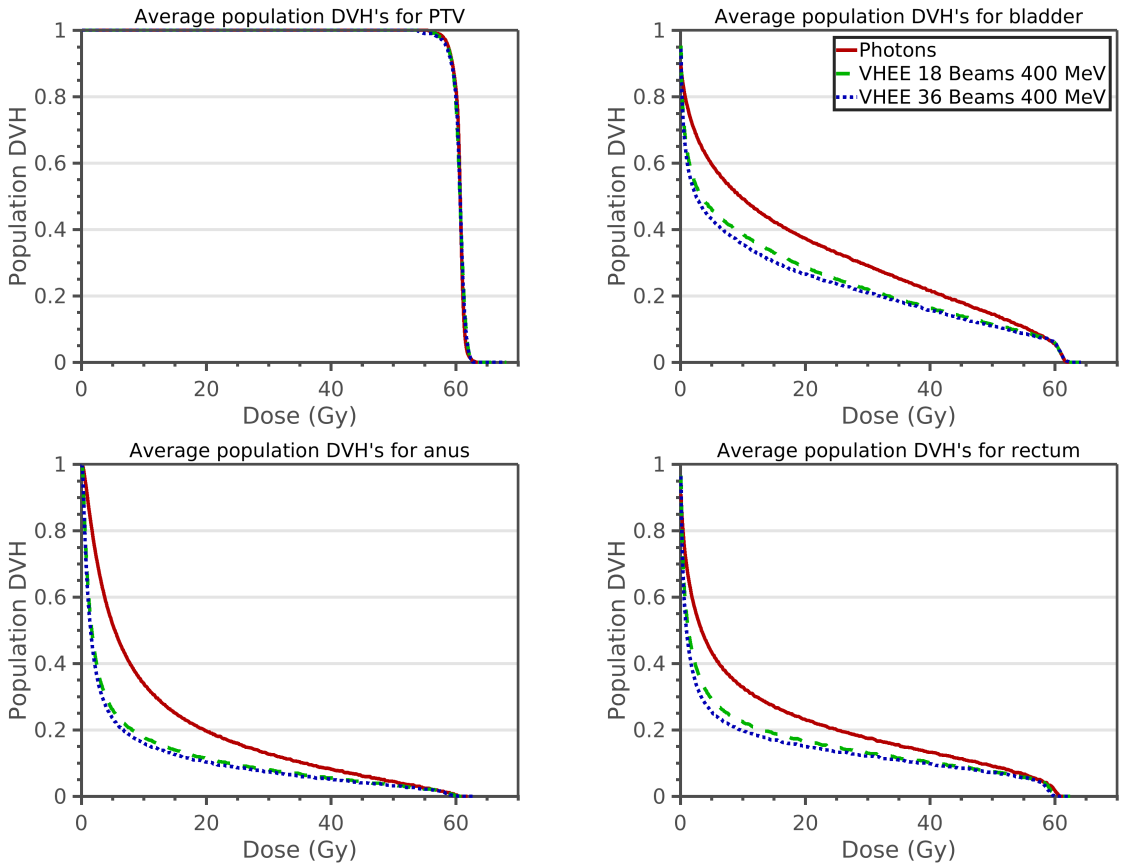

Figure 5.4: Comparisons of population-averaged (n=10) dose volume histograms between IMRT treatment plan and the 18-36 beam 400 MeV treatment plans. Graphs of the PTV (red), bladder (light blue), anus (dark blue) and rectum (green).

The most relevant dosimetric parameters are presented in Table 5.1, the table shows the mean value a standard deviation. The IMRT plan is compared with the 9, 18 and 36 beam VHEE treatment plans using a beam energy of 300 MeV. The dosimetric variables are given for the PTV, rectum, patient, anus, bladder and femur heads.

The rectum receives a similar mean dose with the 9 beam and IMRT plan. For the 18 and 36 beam plans the D_{mean} reduces from 13.4 Gy to 11.1 Gy (p = 0.002) and 9.9 Gy (p = 0.002).

The mean dose to the anus is reduced from 12.4 Gy for the IMRT plan to 10.6 Gy (p=0.014), 8.7 Gy (p=0.002) and 8.0 Gy (p=0.002) for the 9, 18 and 36 beam treatment plans. Comparing the IMRT plan mean bladder dose to the VHEE plans shows a reduction in dose from 20.1 Gy to 18.0 Gy (p=0.002), 16.8 Gy (p=0.002) and 15.8 Gy (p=0.002) for the 9, 18 and 36 beam treatment plans.

The right femoral head dose increased from the IMRT 27.8 Gy to 30.1 Gy (p=0.004) and 29.5 Gy (p=0.037) for the 9 and 18 beam treatment plans. The left femorla head maximum dose increases from 28.5 Gy for IMRT to 30.3 (p=0.01) for 9 beam VHEE.

Table 5.1: Dose metrics comparing 23 beam IMRT with 9, 18 and 36 Beam VHEE treatment plans with 300 MeV. Table shows mean values with 1 sigma standard deviation for metrics (n=10). Results are shown for PTV, rectum, anus, bladder, left femur head (LFH), right femur head (RFH), the complete patient and p-values for t-test between IMRT and the three VHEE plans.

			Beams			p-values		
		IMRT	9	18	36	IMRT - 9 Beams	IMRT - 18 Beams	IMRT - 36 Beams
PTV	$V_{57Gy}(\%)$	99.9 ± 0.04	99.9 ± 0.04	99.9 ± 0.04	99.8 ± 0.05	0.049	0.014	0.002
	$V_{64,2Gy}(\%)$	0.0	0.0	0.0	0.0	-	-	-
	$D_{0.001cc}(Gy)$	66.5 ± 0.5	66.1 ± 0.5	66.7 ± 0.6	67.3 ± 0.3	0.064	0.625	0.002
	$D_{mean}(Gy)$	63.5 ± 0.3	63.6 ± 0.5	64.2 ± 0.6	64.6 ± 0.4	0.922	0.004	0.002
	$CI_{95\%}$	1.10 ± 0.02	1.09 ± 0.02	1.10 ± 0.02	1.11 ± 0.01	0.492	0.770	0.105
	$CI_{Riet95\%}$	0.89 ± 0.02	0.90 ± 0.01	0.89 ± 0.02	0.88 ± 0.01	0.432	0.625	0.105
	$CI_{50\%}$	4.84 ± 0.28	4.08 ± 0.31	4.04 ± 0.21	4.15 ± 0.29	0.002	0.002	0.002
Rectum	$D_{mean}(Gy)$	13.4 ± 4.4	14.0 ± 4.0	11.1 ± 3.9	9.9 ± 3.8	0.375	0.002	0.002
	$V_{58Gy}(\%)$	6.5 ± 3.6	6.4 ± 3.4	6.0 ± 3.3	6.0 ± 3.3	1.000	0.002	0.002
	$V_{50Gy}(\%)$	10.1 ± 4.8	10.1 ± 4.6	8.8 ± 4.3	8.4 ± 4.2	0.770	0.002	0.002
Patient	$D_{mean}(Gy)$	4.1 ± 0.7	3.6 ± 0.6	3.6 ± 0.7	3.6 ± 0.6	0.002	0.002	0.002
	$V_{3Gy}(\%)$	23.4 ± 3.0	24.0 ± 3.3	23.5 ± 3.4	22.9 ± 3.3	0.037	0.492	0.131
	$V_{15Gy}(\%)$	10.2 ± 2.0	8.3 ± 1.6	8.0 ± 1.7	7.8 ± 1.7	0.002	0.002	0.002
	$V_{30Gy}(\%)$	2.9 ± 0.7	2.2 ± 0.5	2.3 ± 0.6	2.4 ± 0.6	0.002	0.002	0.002
Anus	$D_{mean}(Gy)$	12.4 ± 4.9	10.6 ± 5.1	8.7 ± 4.5	8.0 ± 4.2	0.014	0.002	0.002
Bladder	$D_{mean}(Gy)$	20.1 ± 11.5	18.0 ± 11.0	16.8 ± 10.5	15.8 ± 10.0	0.002	0.002	0.002
L.F.H.	$D_{0.001cc}(Gy)$	28.5 ± 1.5	30.3 ± 1.2	29.1 ± 2.1	28.1 ± 2.2	0.010	0.375	0.492
R.F.H.	$D_{0.001cc}(Gy)$	27.8 ± 2.2	30.1 ± 1.2	29.5 ± 3.1	28.6 ± 3.0	0.004	0.037	0.193

Table 5.2 shows the significance of differences between VHEE treatment plans, three comparisons were made: 9 to 18 beams, 18 to 36 beams and 36 to 9 beams. The PTV Coverage shows some significant differences in the mean dose between the 9 beam and the 18/36 beam plans despite normalization.

The rectum mean dose reduces with an increasing number of beams in the treatment plan (p=0.002) The same is true for the anus (p=0.002) and bladder dose (p=0.002).

An overview of the average dosimetric parameters comparing IMRT with all the possible VHEE treatment plan variations (electron beam energy and number of beams) can be found in the table of Appendix G.

Table 5.2: Comparison of the significance of differences between dosimetric parameters of VHEE treatment plans.

		p-values		
		9 - 18	18 - 36	36 - 9
PTV	$V_{57Gy}(\%)$	0.0020	0.0020	0.0020
	$D_{0.001cc}(Gy)$	0.0020	0.0645	0.0020
	$D_{mean}(Gy)$	0.0020	0.0840	0.0020
	$CI_{95\%}$	0.0488	0.1055	0.0039
	$CI_{Riet95\%}$	0.0488	0.1055	0.0039
	$CI_{50\%}$	0.6250	0.0371	0.4922
Rectum	$D_{mean}(Gy)$	0.0020	0.0020	0.0020
	$V_{58Gy}(\%)$	0.0020	0.0645	0.0020
	$V_{50Gy}(\%)$	0.0020	0.0020	0.0020
Patient	$D_{mean}(Gy)$	1.0000	0.2324	0.2754
	$V_{3Gy}(\%)$	0.0020	0.0098	0.0039
	$V_{15Gy}(\%)$	0.0020	0.0645	0.0039
	$V_{30Gy}(\%)$	0.0371	0.0059	0.0059
Anus	$D_{mean}(Gy)$	0.0020	0.0020	0.0020
Bladder	$D_{mean}(Gy)$	0.0020	0.0020	0.0020
L.F.H.	$D_{0.001cc}(Gy)$	0.0645	0.1055	0.0098
R.F.H.	$D_{0.001cc}(Gy)$	0.6250	0.0371	0.1309

5.2. Comparing treatment plans with 200,300 and 400 MeV

This section examines the effects of electron energy on the quality of the treatment plan. The IMRT treatment plan is compared with 200, 300 and 400 MeV VHEE treatment plans. The axial dose distribution and dosimetric parameters are presented for the VHEE treatment plans with 18 beams and the DVHs are shown for 9, 18 and 36 beams.

The lateral dose distribution for IMRT and the VHEE plans are shown in Figure 5.5. The clear pencil beam lines are visible in all VHEE plans, although they are less apparent for the 400 MeV plan.

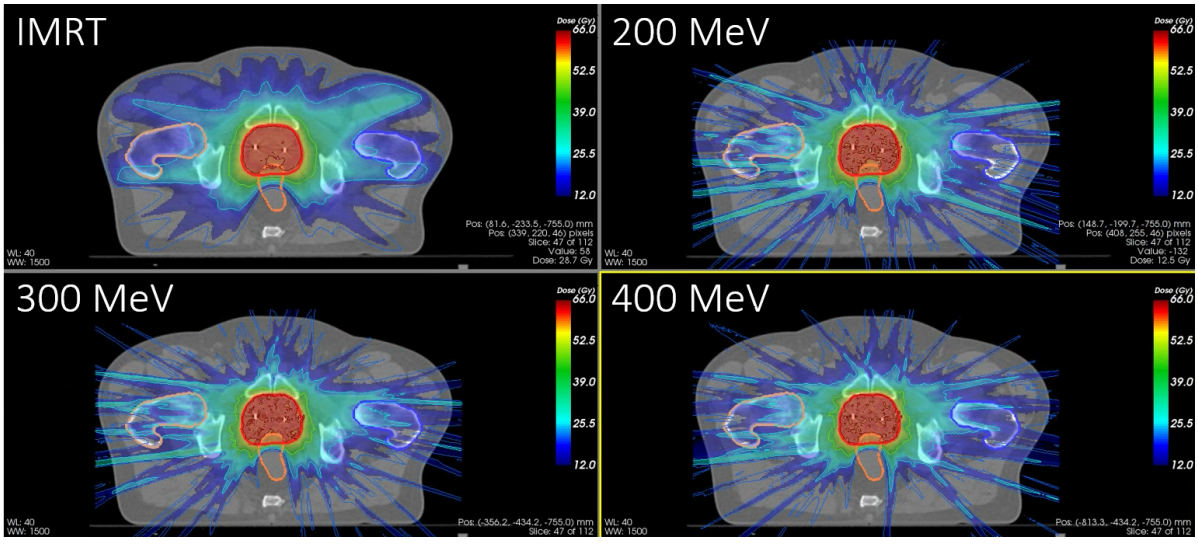

Figure 5.5: Axial dose distribution for Patient 6. Comparing IMRT with 36 equiangular spaced beams of 200, 300 and 400 MeV.

The average population DVHs comparing different electron energies for the PTV, bladder, anus and rectum are shown in Figures 5.6 to 5.8. The plans show no significant differences in the PTV coverage. Figure 5.7 shows the treatment plans with 18 beams and this shows that the quality of the 200 MeV plan is similar to the IMRT plan. With increasing energy the VHEE treatment plans perform significantly better in comparison to the IMRT plan. A larger improvement in quality is seen when the energy is increased from 200 to 300 MeV in comparison to the increase from 300 to 400 MeV.

Figure F.1 in the appendix presents the DVHs for all patients. The DVHs for the 23 beam IMRT plan are compared with the 200, 300 and 400 MeV 18 beam plans. When the electron beam energy was increased the quality of the plan improved for all patients. The patient dose is superior for IMRT plans below 3 Gy and inferior above 3 Gy when compared to the VHEE plans.

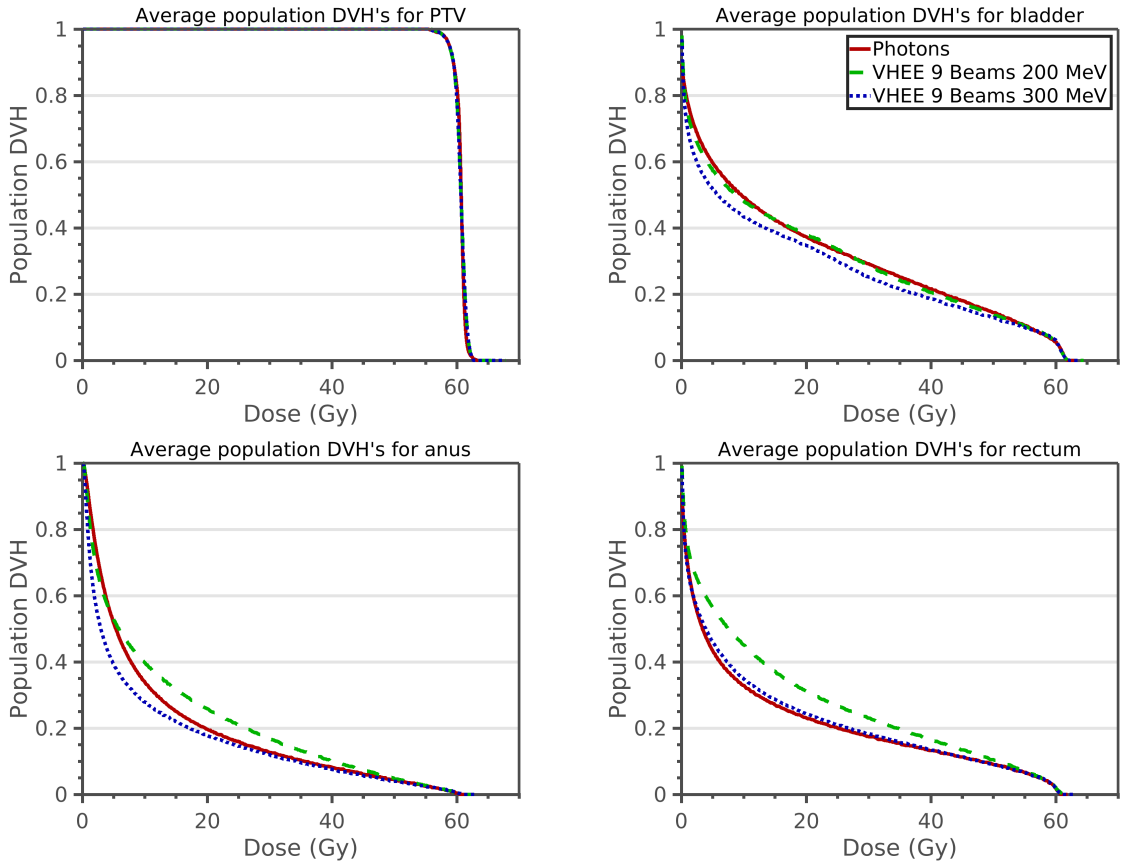

Figure 5.6: Comparisons of population-averaged (n=10) dose volume histograms between IMRT treatment plan and the 200-300 MeV treatment plans for 9 beams. Graphs of the PTV (red), bladder (light blue), anus (dark blue) and rectum (green).

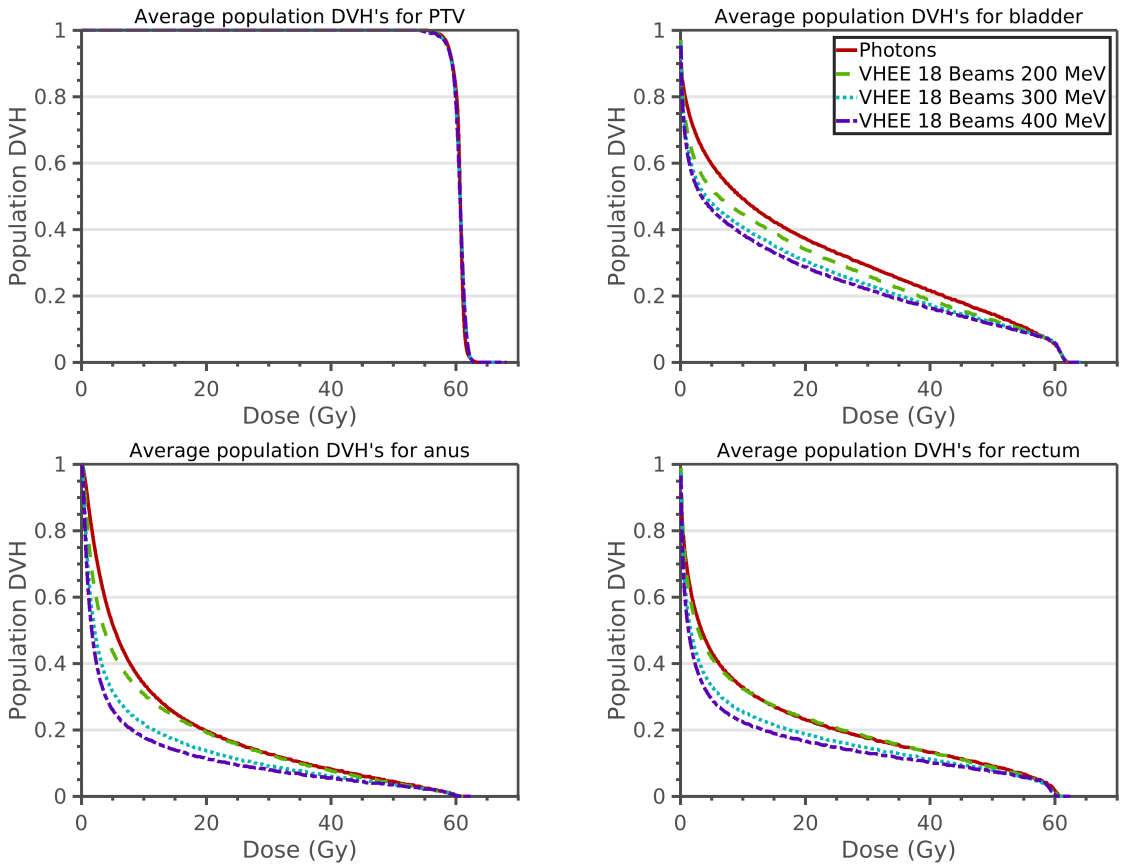

Figure 5.7: Comparisons of population-average dose volume histograms (n=10) between IMRT treatment plan and the 200-300-400 MeV treatment plans for 18 beams. Graphs of the PTV (red), bladder (light blue), anus (dark blue) and rectum (green).

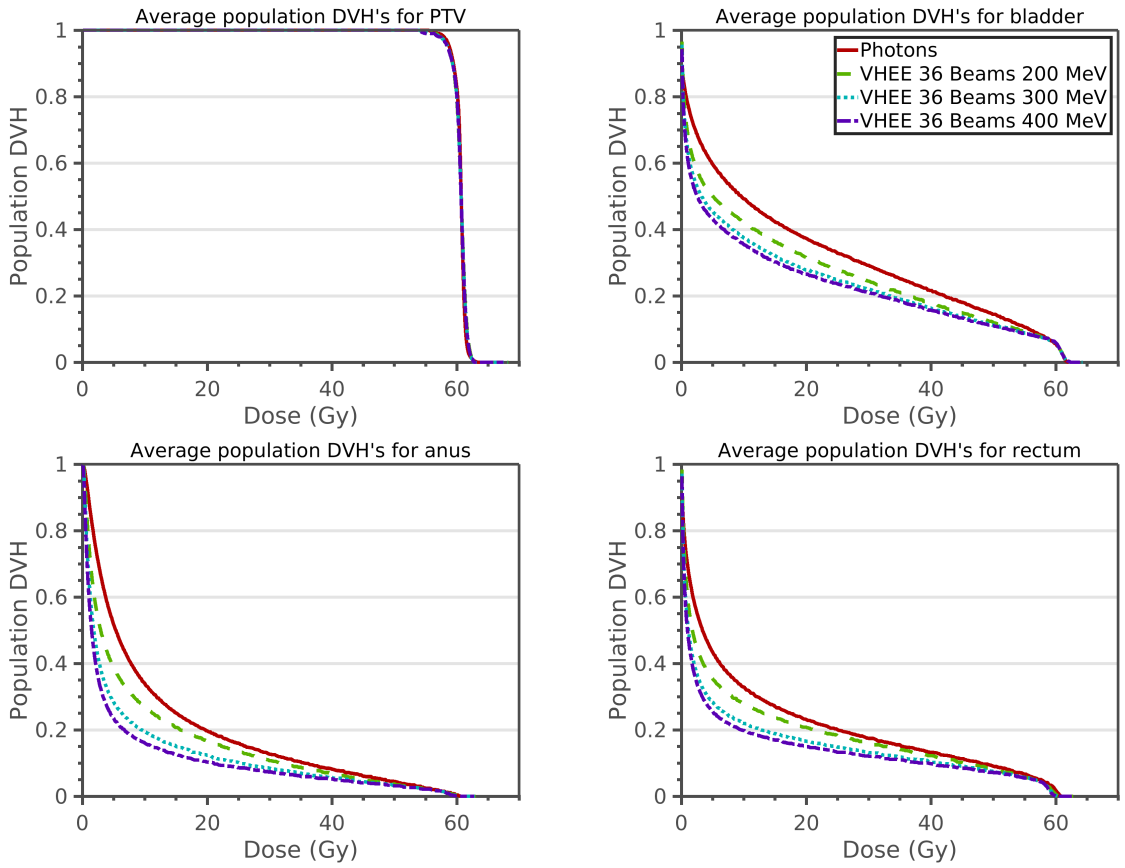

Figure 5.8: Comparisons of population-averaged (n=10) dose volume histograms between IMRT treatment plan and the 200-300-400 MeV treatment plans for 36 beams. Graphs of the PTV (red), bladder (light blue), anus (dark blue) and rectum (green).

Table 5.3 lists the most relevant dosimetric variables, the table shows the mean value and a standard deviation. The IMRT treatment plan is compared with the 200, 300 and 400 MeV treatment plans using 18 beams. The dosimetric variables are given for the PTV, rectum, patient, anus, bladder and femur heads.

The rectum receives a similar mean dose in the 200 MeV plan compared with IMRT plan. For the 300 and 400 MeV plans the D_{mean} reduces with 2.4 Gy (p=0.002) and 3.5 Gy (p=0.002).

The mean anus dose is comparable between IMRT and 200 MeV plans, the dose is reduced with 3.7 Gy (p=0.002) and 4.9 Gy (p=0.002) for the 300 and 400 MeV plans. The mean bladder dose is lower for all VHEE plans compared to the IMRT plans. The reduction in dose is 1.9 Gy (p=0.002), 3.3 Gy (p=0.002) and 4.2 Gy (p=0.002) for the 200, 300 and 400 MeV plans.

Table 5.3: Dose metrics comparing 23 beam IMRT with VHEE 200, 300 and 400 MeV treatment plans with 18 beams. Table shows mean values with 1 sigma standard deviation for metrics (n=10). Results are shown for PTV, rectum, anus, bladder, left femur head (LFH), right femur head (RFH), the complete patient and p-values for t-test between IMRT and the three VHEE plans.

			Energy			p-values		
		IMRT	200 MeV	300 MeV	400 MeV	IMRT - 200 MeV	IMRT - 300 MeV	IMRT - 400 MeV
PTV	$V_{57Gy}(\%)$	99.9 ± 0.04	99.9 ± 0.03	99.9 ± 0.04	99.8 ± 0.07	0.193	0.010	0.004
	$V_{64,2Gy}(\%)$	0.0	0.0	0.0	0.0	-	-	-
	$D_{0.001cc}(Gy)$	66.5 ± 0.5	66.3 ± 0.3	66.7 ± 0.6	66.8 ± 0.4	0.275	0.557	0.084
	$D_{mean}(Gy)$	63.6 ± 0.3	63.8 ± 0.3	64.2 ± 0.6	64.3 ± 0.4	0.064	0.006	0.004
	$CI_{95\%}$	1.10 ± 0.03	1.09 ± 0.01	1.10 ± 0.02	1.11 ± 0.02	0.193	0.695	0.232
	$CI_{Riet95\%}$	0.89 ± 0.02	0.90 ± 0.01	0.89 ± 0.02	0.89 ± 0.01	0.232	0.625	0.232
	$CI_{50\%}$	4.84 ± 0.28	4.20 ± 0.27	4.04 ± 0.21	3.97 ± 0.22	0.002	0.002	0.002
Rectum	$D_{mean}(Gy)$	13.5 ± 4.4	13.4 ± 4.3	11.1 ± 3.9	10.0 ± 3.6	0.770	0.002	0.002
	$V_{58Gy}(\%)$	6.5 ± 3.6	6.2 ± 3.4	6.0 ± 3.3	6.0 ± 3.3	0.006	0.002	0.002
	$V_{50Gy}(\%)$	10.2 ± 4.8	9.9 ± 4.9	8.8 ± 4.3	8.3 ± 4.2	0.160	0.002	0.002
Patient	$D_{mean}(Gy)$	4.1 ± 0.7	3.7 ± 0.6	3.6 ± 0.7	3.6 ± 0.7	0.002	0.002	0.002
	$V_{3Gy}(\%)$	23.4 ± 3.0	23.8 ± 3.2	23.5 ± 3.4	23.1 ± 3.2	0.105	0.492	0.322
	$V_{15Gy}(\%)$	10.2 ± 2.0	8.3 ± 1.7	8.0 ± 1.7	7.8 ± 1.7	0.002	0.002	0.002
	$V_{30Gy}(\%)$	2.9 ± 0.7	2.3 ± 0.6	2.3 ± 0.6	2.3 ± 0.6	0.002	0.002	0.002
Anus	$D_{mean}(Gy)$	12.4 ± 4.9	11.4 ± 5.1	8.7 ± 4.5	7.5 ± 4.1	0.160	0.002	0.002
Bladder	$D_{mean}(Gy)$	20.1 ± 11.5	18.2 ± 11.0	16.8 ± 10.5	15.9 ± 9.9	0.002	0.002	0.002
L.F.H.	$D_{0.001cc}(Gy)$	28.5 ± 1.5	28.4 ± 2.0	29.1 ± 2.1	28.8 ± 2.3	0.695	0.492	0.846
R.F.H.	$D_{0.001cc}(Gy)$	27.8 ± 2.2	28.0 ± 2.9	29.4 ± 3.1	29.6 ± 2.8	1.000	0.037	0.006

The VHEE treatment plans are comapred by t-test in Table 5.4. The PTV coverage shows some significant differences in the mean dose between 200 and the 300/400 plans despite normalization. The rectum mean dose reduces from 200 to 400 MeV (p=0.002). The anus and bladder dose reduces with increasing beam energy (p=0.002).

Table 5.4: Comparison of the significance of differences between dosimetric parameters of VHEE treatment plans.

		p-values		
		200 - 300	300 - 400	400 - 200
PTV	$V_{57Gy}(\%)$	0.0020	0.0039	0.0020
	$D_{0.001cc}(Gy)$	0.0039	0.0840	0.0020
	$D_{mean}(Gy)$	0.0020	0.1055	0.0020
	$CI_{95\%}$	0.0020	0.1055	0.0020
	$CI_{Riet95\%}$	0.0020	0.1055	0.0020
	$CI_{50\%}$	0.0020	0.0273	0.0020
Rectum	$D_{mean}(Gy)$	0.0020	0.0020	0.0020
	$V_{58Gy}(\%)$	0.0039	0.1602	0.0020
	$V_{50Gy}(\%)$	0.0020	0.0020	0.0020
Patient	$D_{mean}(Gy)$	0.0020	0.0039	0.0020
	$V_{3Gy}(\%)$	0.1055	0.0098	0.0195
	$V_{15Gy}(\%)$	0.0039	0.0195	0.0020
	$V_{30Gy}(\%)$	0.0137	0.1602	0.0059
Anus	$D_{mean}(Gy)$	0.0020	0.0020	0.0020
Bladder	$D_{mean}(Gy)$	0.0020	0.0020	0.0020
L.F.H.	$D_{0.001cc}(Gy)$	0.1055	0.9219	0.3750
R.F.H.	$D_{0.001cc}(Gy)$	0.0020	0.1934	0.0488

5.3. Combined 200/300 MeV Treatment plan

Combining energies might result in lower patient doses due to selection of a beam energy with the PDD peak in the PTV.

The average population DVHs are shown in Figure 5.9. The DVHs of the combined 200/300 MeV plans are compared with the 18 and 36 beam 300 MeV plans. The combined plan contains 18 beams with both 200 MeV and 300 MeV pencil beams. No difference was found in PTV coverage.

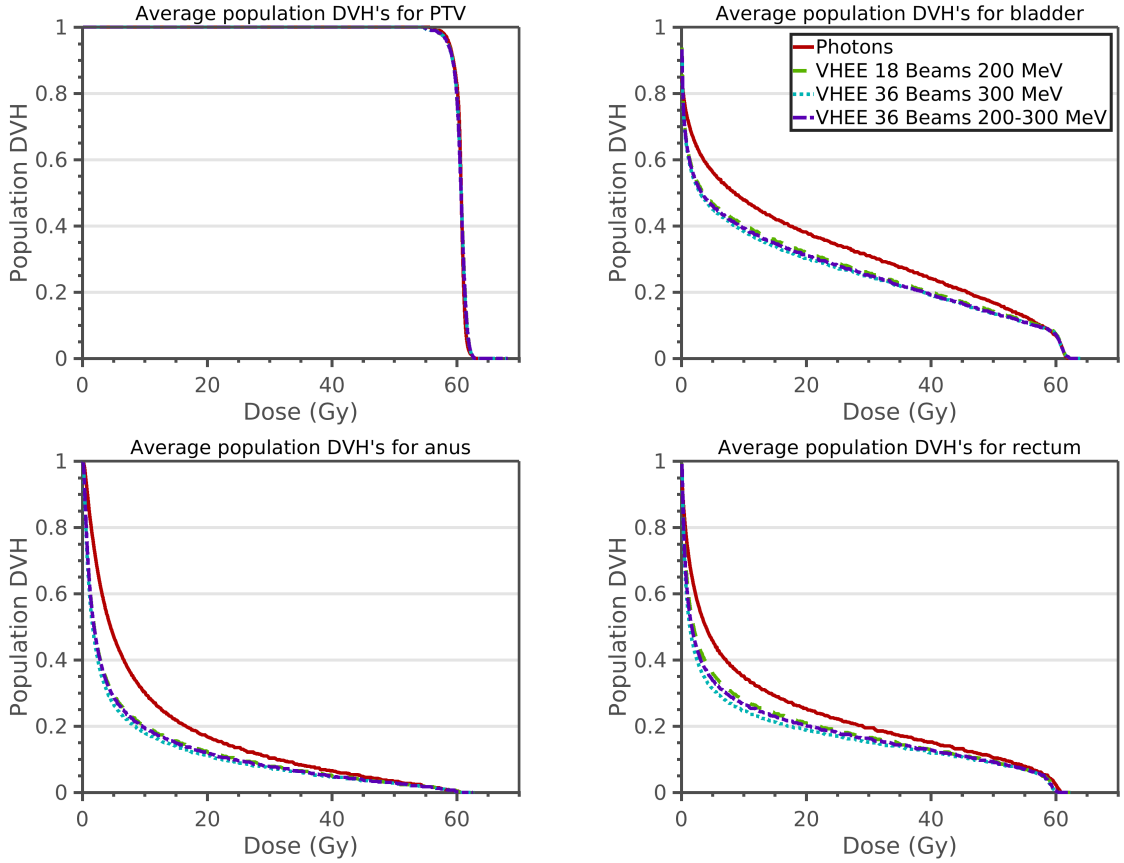

Figure 5.9: Comparisons of population-averaged (n=6) dose volume histograms between Combined 200/300 MeV treatment plan and the 18 and 36 beam 300 MeV treatment plans. Graphs of the PTV (red), bladder (light blue), anus (dark blue) and rectum (green).

For the bladder all plans have a similar DVH graph, but the 36 beam 300 MeV plan is at least similar to the combined plan.

The 36 beam 300 MeV plan is better at healthy tissue saving in the rectum and anus compared to the combined plan. The 18 beam plan is similar to the combined beam plan.

5.4. Computational performance

Computations for TOPAS MC calculations were performed on the TU Delft High-Performance computing cluster 11. The calculations utilized 8 CPUs. The mean runtime for a single beam calculation was 6.7 hours with a standard deviation (SD) of 4.0 hours. On average $5.0 \cdot 10^6$ particles with a SD of $9.2 \cdot 10^5$ were used for each beam. This value changes based on the number of pencil beams. Performance calculations are based on 652 simulations.

Optimizations were performed on the Uluru computing cluster of the Erasmus MC. Simulations were allocated 8 CPUs from one node and 70 GB of RAM memory. The mean runtime for a sample size of 20 simulations is shown in Table 5.5. The 20 simulations contain a random distribution of the three energy levels.

Table 5.5: Computational performance of Erasmus-iCycle optimization for 9, 18 and 36 beam plans. The runtime average and standard deviation is shown in hours for 20 simulations.

	9 Beams	18 Beams	36 Beams
Runtime (hours)	1.6	5.1	20.3
Standard deviation (hours)	0.56	1.57	5.6

6

Discussion

This thesis presents treatment plans for radiotherapy with very high energy electrons compared with IMRT treatment plans. Monte Carlo simulations for 10 prostate cancer patients were calculated using 36 equiangular spaced beams for 200, 300 and 400 MeV. Treatment plans with 9, 18 and 36 beams were created and optimized for each of these energy levels.

6.1. Comparison of VHEE and IMRT treatment plans

VHEE treatment plans can reduce the dose to organs at risk (OAR), while maintaining a similar PTV coverage as IMRT treatment plan. Only the 9 and 18 beam 200 MeV treatment plans performed similar or worse to the IMRT treatment plan. The other VHEE treatment plans reduced the dose in all OAR except for the femoral heads.

The treatment plans were normalized for PTV coverage. Small deviations in the PTV coverage were seen in the 36 beam treatment plans for 200 MeV (p=0.004) and 300 MeV (p=0.014) despite normalization. This lower PTV coverage can lead to greater reduction in the OAR dose and in this way can make it more difficult to ensure a fair comparison

The rectum dose is significantly reduced in VHEE treatment plans compared to the IMRT treatment plans. This can be seen in the D_{mean} which reduces from 13.5 Gy for IMRT treatment plan to between 9.2 and 11.9 Gy (p=0.002-0.004) for VHEE treatment plans. Three VHEE treatment plans performed similar or worse than the IMRT plan (9 beam 200 MeV;18 beam 200 MeV;9 beam 300 MeV).

The same pattern is found when comparing the mean anus dose in the IMRT treatment plan and the VHEE treatment plans. For all but two plans a reduction in dose between 1.8 Gy and 5.4 Gy (p=0.002-0.014) was found. When comparing IMRT and VHEE treatment plans for the mean bladder dose a reduction in dose between 1.9 and 4.9 Gy (p=0.002) was found for all but one VHEE treatment plan.

The mean patient dose is reduced in the VHEE treatment plans (p=0.002), The $V_{15\%}$ and $V_{30\%}$ are also reduced (p=0.002). The $V_{3\%}$ is not significantly different between most VHEE treatment plans and the IMRT plan.

The VHEE treatment plans were either similar in quality or worse when comparing the dose to the femoral heads. The left femoral head $D_{0.001cc}$ showed only a significant increase in dose for one VHEE plan(p=0.01). The right femoral head $D_{0.001cc}$ is greater for three VHEE treatment plans compared to IMRT (p=0.004-0.037). The increase in dose is between 1.7 Gy and 2.3 Gy.

When comparing the VHEE treatment plans with at least 18 beams and 300 MeV beam energy to IMRT a strong reduction in dose to OAR is seen, except for the femoral heads.

Literature on prostate cancer treatment with VHEE is consistent with our conclusion that VHEE reduces the mean OAR dose, while maintaining a similar PTV coverage. Fuchs et al. [13] compared 7 beam 150 and 250 MeV VHEE treatment plans with 6 MV IMRT treatment plans. The article calculated the treatment plans for one patient with a prescribed gross tumor dose of 76 Gy. The PTV coverage was found to be comparable for all treatment plans. The mean doses to the rectum, bladder and normal tissue were reduced with VHEE treatment plans. The rectum mean dose were found to be 39.6 Gy for the IMRT plan, 37.8 for the 150 MeV plan and 34.7 for the 250 MeV plan. The bladder mean dose for

the IMRT, 150 MeV and 250 MeV plans was found to be 39.1, 35.8 and 32.7 Gy. Normal tissue mean dose was 16.7 Gy for the IMRT plan and 14.5 and 14.1 Gy for the 150 and 250 MeV plans.

Comparing VHEE with VMAT for one patient has been performed by Bazalova-Carter et al. [4]. The prostate was treated with a two-arc 15 MV VMAT therapy and the VHEE treatment plan used a 100 MeV electron beam and 36 beams. Both plans irradiated the 95% of the PTV with 78 Gy. The PTV coverage was similar for both treatment plans with $CI_{100\%}$ of 1.04 and 1.03 for the VHEE and VMAT plans. The dose mean dose to the bladder, rectum and normal tissue was lower in the VHEE treatment plans. The difference was small and mostly in the lower dose region.

Schüler et al. [39] generated a 76 Gy 200 MeV VHEE treatment plan and VMAT plan for one patient. The Conformality Index for the VMAT was 1.00 compared so performed better compared to 1.06 for the VHEE treatment plan. The OAR received a lower dose with bladder dose being reduced by 1% and the rectum dose by 13%.

6.2. Influence of the number of beams

Increasing the number of beams per treatment plan reduces the mean dose to the OAR while the PTV dose conformity remains similar. This trend was found for all the different beam energies and holds true for all patients.

This pattern can be seen in the mean rectum dose in the 300 MeV treatment plans whereby the doses reduces from 14.0 Gy to 11.1 Gy and 9.9 Gy (9 beam to 18 beam p=0.002, 9 beam to 36 beam p=0.002). The mean bladder dose follows the same pattern with reductions in dose of 1.2 Gy (p=0.002 and 1.0 Gy (p=0.002). The mean anus dose reduces with increasing number of beams in the treatment plans (p=0.002). The V_{3Gy} and V_{15Gy} for the patient decrease slightly when using more beams (p=0.002-0.0039), but the V_{30Gy} slightly increases with more beams in the treatment plans (p=0.0059-0.0371). The femoral heads maximum dose shows no clear pattern when the number of beams is increased.

6.3. Influence of the electron beam energy

Comparing 200, 300 and 400 MeV treatment plans shows that higher energies result in lower doses to the OAR.

This reduction was found in the mean rectum dose with a reduction of 2.4 Gy (p=0.002) and 3.4 Gy (p=0.002) whe the 200 MeV 18 beam treatment plan was compared with the 300 and 400 MeV treatment plans. The mean anus dose reduces from 11.4 Gy to 8.7 Gy (p=0.002) and 7.5 Gy (p=0.002). The same pattern is found in the mean bladder dose with 18.2 Gy, 16.8 Gy (p=0.002) and 15.9 Gy (p=0.002). The dose in the OAR reduces when the beam energy is increased, except for the femoral heads.

6.4. Further work

VHEE is a potential replacement for IMRT treatment of prostate cancer because of the reduced dose to healthy tissue, while maintaining a similar PTV coverage. When the number of beams in a treatment plan is increased the dose to the OAR is reduced. Increasing the beam energy also reduces the dose to the OARs. There are a number of items to consider for further research.

Simulations were limited to 200, 300 and 400 MeV electron beams. Treatment plans with higher energies could exceed the plan quality of these 200 MeV to 400 MeV treatment plans. The penumbra of a higher energy electron beam is smaller and remains small while in the patient. This could potentially further reduce the dose to the OARs.

Optimization for this project was limited due to memory constraints in MATLAB. Increasing the voxel sampling during the treatment plan optimization phase could improve VHEE treatment plans by reducing single high dose pencil beams.

The tumor depth from the surface of the patient depends on the radiation direction. Using multiple energies could allow for utilization of the difference in depth dose curves and potentially improving treatment plan quality. Combining beams of multiple energies has been tried and was found not to be beneficial, but the difference between the energies was very small and not optimized. Comparison of treatment plans with a greater energy difference could be useful.

Beam angle selection is an important part of treatment plan optimization. Determining the optimal configuration and number of beams for a patient could improve the plan quality.

This thesis project focused solely on prostate cancer. An interesting topic for further research would be to compare VHEE and IRMT as treatment modalities for other types of cancer for example lung cancer.
There are a couple of restrictions on VHEE therapy. VHEE beams result in a relative high dose to the skin compared to photon beams. Combining VHEE and treatment techniques with high single beam dose such as FLASH therapy would probablity exceed dose limits to the skin. In this report VHEE has not been compared to proton therapy, but from the literature it is clear that proton therapy results in much lower OAR dose compared to VHEE.

There is currently no equipment for performing clinical VHEE treatments. Accurate data on potential pencil beam shapes and intensity profiles is not available. Delivery of the pencil beams to a specific location in the patient will most likely be done by electro-magnetic pencil beam scanning. The accuracy and speed of such a system for electrons should be studied and will be important in determining the usefulness of VHEE as a potential clinical treatment modality.

Treatments could potentially be further improved by magnetic focusing of electron beams, as illustrated by Kokurewicz et al. [20]. These are pencil beams with a focus point inside of the patient at the tumor depth. This might be beneficial in two ways: the focused spot will have a high peak dose and the focal spot size will be smaller when compared to unfocused beams.

Appendices

Appendix A: Workflow VHEE

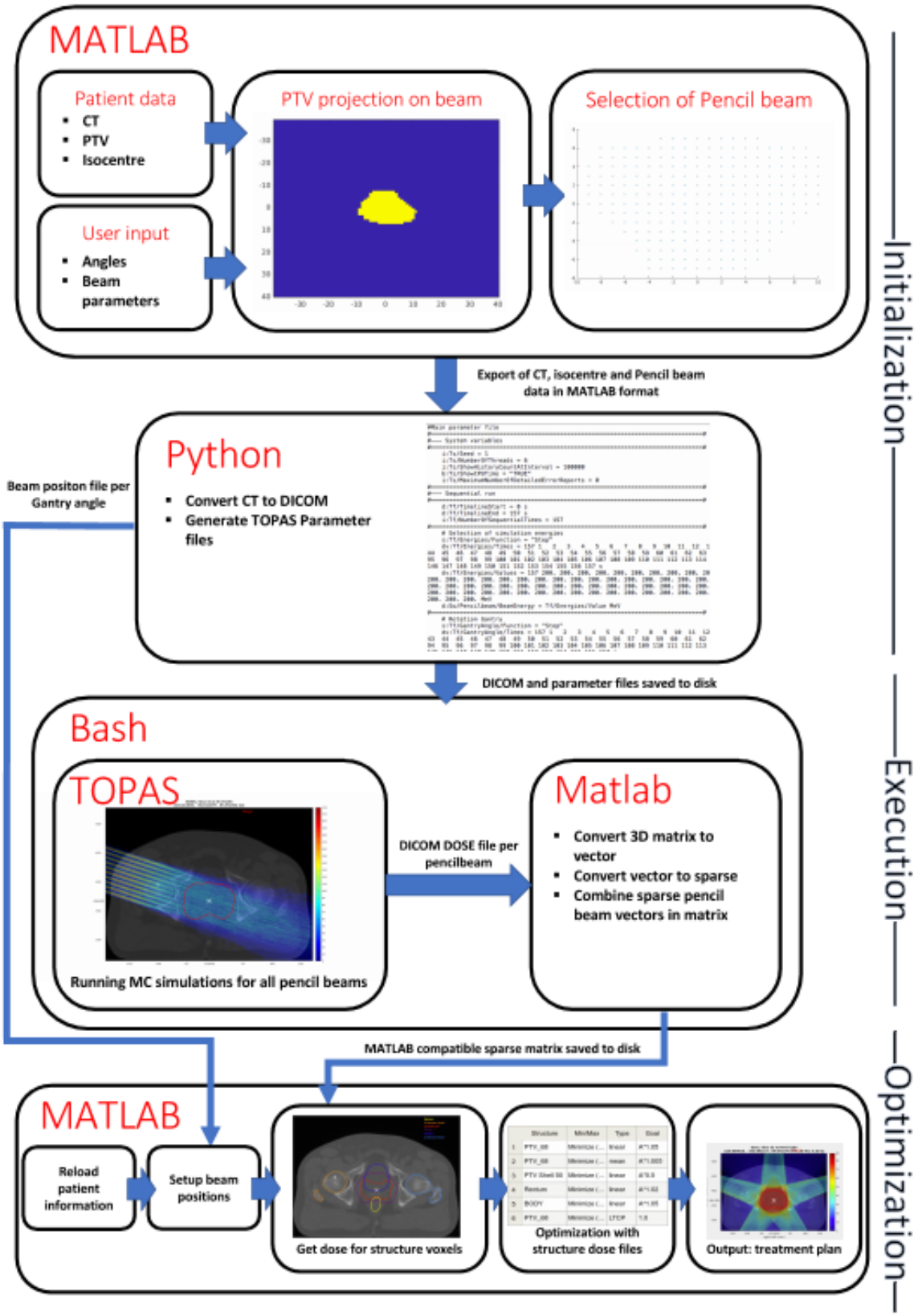

Figure A.1: Flowchart for generation of a VHEE treatment plan using Monte Carlo simulator TOPAS and optimization MATLAB package Erasmus-iCycle.

Appendix B: Wishlist iCycle

Prescribed dose A: 60.0000 B: 0.0000 C: 0.0000

	Structure	Min/Max	Type	Goal	Limit	Sufficient	Priority	Weight	Parameters	
1	PTV_6000	Minimize (maximum) ⇩	linear	A*1.05			Constraint	1		Yes
2	Patient	Minimize (maximum) ⇩	linear	A*1.05			Constraint	1		Yes
3	PTV_ring_5cm	Minimize (maximum) ⇩	linear	A*0.5			Constraint	1		Yes
4	PTV_6000	Minimize (maximum) ⇩	LTCP	0.7		0.7	1	1	A*0.99 0.9	Yes
5	PTV_6000	Minimize (maximum) ⇩	mean	A*1.01			Constraint	1		Yes
6	PTV_Shell_5	Minimize (maximum) ⇩	linear	A*0.85			4	1		Yes
7	PTV_ring_1cm	Minimize (maximum) ⇩	linear	0.6*A			6	1		Yes
8	PTV_ring_3cm	Minimize (maximum) ⇩	linear	0.3*A			6	1		Yes
9	Rectum	Minimize (maximum) ⇩	linear	58			4	1		Yes
10	Rectum	Minimize (maximum) ⇩	mean	5			5	1		Yes
11	Rectum	Minimize (maximum) ⇩	EUD	30			2	1	12	Yes
12	Rectum	Minimize (maximum) ⇩	EUD	20			3	1	8	Yes
13	Anus	Minimize (maximum) ⇩	mean	5			5	1		Yes
14	Anus	Minimize (maximum) ⇩	mean	35			Constraint	1		Yes
15	Femur_Head_L	Minimize (maximum) ⇩	linear	40			Constraint	1		Yes
16	Femur_Head_L	Minimize (maximum) ⇩	linear	25			8	1		Yes
17	Femur_Head_R	Minimize (maximum) ⇩	linear	40			Constraint	1		Yes
18	Femur_Head_R	Minimize (maximum) ⇩	linear	25			8	1		Yes
19	Bladder	Minimize (maximum) ⇩	mean	5			7	1		Yes
20	PTV_ring_1cm	Minimize (maximum) ⇩	linear	A*0.85			Constraint	1		Yes
21	ExternalRing	Minimize (maximum) ⇩	linear	0.5*A			Constraint	1		Yes
22	ring_5cm_tot_external	Minimize (maximum) ⇩	linear	0.7*A			Constraint	1		Yes
23	Smoothing 1st	Minimize (maximum) ⇩	linear	10*A			Constraint	1		Yes
24	Smoothing 1st	Maximize (minimum) ⇧	linear	-10*A			Constraint	1		Yes
25	Smoothing 2nd	Minimize (maximum) ⇩	quadratic	0.6*0.6*10*A*A			Constraint	1		Yes

Figure B.1: Wishlist containing cnstraints and objectives for iCycle optimization. Structures are the PTV, patient, rectum, anus, femur left and right and bladder. Additionaly structures are rings around the PTV and 5 cm ring along the edge of the patient. Objectives are to minimize the maximum by either linear, LTCP, mean or EUD optimization. A is a variable with valume 60 Gy. Figure extracted from lucy part of the Erasmus-iCycle from ERASMUS MC.

	Assign To	Structre 1	Operation	Structure 2	Parameters
1	ExternalRing	Patient	Ring Inside		20
2	PTV_ring_1cm	PTV+2cm	Subtract	PTV+1cm	
3	PTV_ring_3cm	PTV+3cm	Subtract	PTV+2cm	
4	PTV_ring_5cm	PTV+5cm	Subtract	PTV+3cm	
5	ring_5cm_tot_external	Patient	Subtract	PTV+5cm	
6	PTV_Shell_5	PTV_6000	Shell		5

Figure B.2: Table containing all additionaly volumes. ExternalRing is a ring inside the patient of 20 millimeter, moving inwards from the skin. The remaining volumes form rings around the PTV up to the skin. The parameter is defined in millimeters.

Appendix C: TOPAS pencil beam

Pencil beam parameter file for TOPAS MC. Contains the variables used for the pencil beam in all simulations. Parameters are based on literature study findings.

```
#Pencilbeam
s:So/Pencilbeam/Type = ”Beam”
s:So/Pencilbeam/Component = ”BeamPosition”
s:So/Pencilbeam/BeamParticle = ”e-”
u:So/Pencilbeam/BeamEnergySpread = 0.5
s:So/Pencilbeam/BeamPositionDistribution = ”Gaussian”
s:So/Pencilbeam/BeamPositionCutoffShape = ”Ellipse”
d:So/Pencilbeam/BeamPositionCutoffX = 10 cm
d:So/Pencilbeam/BeamPositionCutoffY = 10 cm
d:So/Pencilbeam/BeamPositionSpreadX = 0.1 cm
d:So/Pencilbeam/BeamPositionSpreadY = 0.1 cm
s:So/Pencilbeam/BeamAngularDistribution = ”Gaussian”
d:So/Pencilbeam/BeamAngularCutoffX = 200. mrad
d:So/Pencilbeam/BeamAngularCutoffY = 200. mrad
d:So/Pencilbeam/BeamAngularSpreadX = 3 mrad
d:So/Pencilbeam/BeamAngularSpreadY = 3 mrad
```

Appendix D: TOPAS main code

Code for simulations of pencil beams using TOPAS MC. Requires the Appendix C code as includeFile, and HUtoMaterialSchneider the default TOPAS converter of CT values to TOPAS material values.

```
#Main parameter file
#=====================================================================#
#--- System variables
#=====================================================================#
    i:Ts/Seed  = 0
    i:Ts/NumberOfThreads  = 10
    i:Ts/ShowHistoryCountAtInterval = 100000
    b:Ts/ShowCPUTime = ”TRUE”
    i:Ts/MaximumNumberOfDetailedErrorReports = 0
#=====================================================================#
#--- Sequential run
#=====================================================================#
    d:Tf/TimelineStart  = 0 s
    d:Tf/TimelineEnd  = 1 s
    i:Tf/NumberOfSequentialTimes  = 1

    # Selection of simulation energies
    d:So/Pencilbeam/BeamEnergy  = 200.0 MeV

    #Scanning of the beam in x-direction
    s:Tf/Gantryscananglex/Function = ”Step”
    dv:Tf/Gantryscananglex/Times  = 1 1 s
    dv:Tf/Gantryscananglex/Values  =1 1 deg

    #Scanning of the beam in y-direction
    s:Tf/Gantryscanangley/Function = ”Step”
    dv:Tf/Gantryscanangley/Times  = 1 1 s
    dv:Tf/Gantryscanangley/Values  = 1 1 deg
#=====================================================================#
#--- Physics
#=====================================================================#
   sv:Ph/Default/Modules = 6 ”g4em-livermore” ”g4h-phy_QGSP_BIC_HP” ”g4decay”
”g4ion-binarycascade” ”g4h-elastic_HP” ”g4stopping”
    d:Ph/Default/EMRangeMin = 100. eV
    d:Ph/Default/EMRangeMax = 500. MeV
#=====================================================================#
#--- Geometry
#=====================================================================#
    d:Ge/GantryR    = 500.0 mm

    #Isocenter of MRI offset
    d:IsoCenterX  = 7.339062500000011 mm
    d:IsoCenterY  = -10.967187499999994 mm
    d:IsoCenterZ  = 16.25 mm

    s:Ge/World/Material = ”Air”
    d:Ge/World/HLX = 1. m
    d:Ge/World/HLY = 1. m
    d:Ge/World/HLZ = 1. m
```

```
    b:Ge/World/Invisible = ”True”

    #Gantry is a cylindrical object around patient to filled with air, and
used by BeamPosition to rotate at 50 cm from center of patient.
    s:Ge/Gantry/Type = ”Group”
    s:Ge/Gantry/Parent = ”World”
    d:Ge/Gantry/TransX = 0. cm
    d:Ge/Gantry/TransY = 0. cm
    d:Ge/Gantry/TransZ = 0. cm
    d:Ge/Gantry/RotX = 0 deg #Tf/Gantryscananglex/Value deg
    d:Ge/Gantry/RotY = 0 deg #Tf/Gantryscanangley/Value deg
    d:Ge/Gantry/RotZ  = 0.0 rad
#=========================================================================#
#--- Beam
#=========================================================================#
    #Beam Position used to laterally move the beam with regards to gantry
rastering
    s:Ge/BeamPosition/Parent = ”Gantry”
    s:So/BeamPosition/Component = ”Gantry”
    d:Ge/BeamPosition/TransX = 0 mm
    d:Ge/BeamPosition/TransY = Ge/GantryR cm
    d:Ge/BeamPosition/TransZ = 0 mm
    d:Ge/BeamPosition/RotX = Tf/Gantryscanangley/Value - 90. deg
    d:Ge/BeamPosition/RotY = Tf/Gantryscananglex/Value deg
    d:Ge/BeamPosition/RotZ = 0 deg
    #Beam contains specifications of the pencil beam design.
    includeFile  = topas_PencilBeam_B1.txt
    i:So/Pencilbeam/NumberOfHistoriesInRun  = 10000
#=========================================================================#
#--- Patients
#=========================================================================#
    includeFile = HUtoMaterialSchneider.txt
    b:Ge/PatientGroup/Include = ”True” # defaults to ”True”
    b:Ge/Patient/Include = ”True” # defaults to ”True”
    s:Ge/PatientGroup/Type   = ”Group”
    s:Ge/PatientGroup/Parent = ”World”
    d:Ge/PatientGroup/TransX = 0 mm
    d:Ge/PatientGroup/TransY = 0 mm
    d:Ge/PatientGroup/TransZ = 0 mm #35. * Ge/VoxelZ cm
    d:Ge/PatientGroup/RotX   = 0. deg
    d:Ge/PatientGroup/RotY   = 0.  deg
    d:Ge/PatientGroup/RotZ   = 0.  deg
    s:Ge/Patient/Parent = ”PatientGroup”
    s:Ge/Patient/Material = ”G4_WATER”
    s:Ge/Patient/Type = ”TsDicomPatient”
    s:Ge/Patient/DicomDirectory  = ”/home/erasmusmc.nl/051097/yartos
    /patients/Patient_Pt006Gr1/TEMP/CT”
    s:Ge/Patient/ImagingToMaterialConverter = ”Schneider”
    iv:Ge/Patient/ShowSpecificSlicesZ = 1 -2
    d:Ge/Patient/RotX = 0. deg
    d:Ge/Patient/RotY = 0. deg
    d:Ge/Patient/RotZ = 90. deg
    dc:Ge/Patient/DicomOriginX = 0. mm
    dc:Ge/Patient/DicomOriginY = 0. mm
    dc:Ge/Patient/DicomOriginZ = 0. mm
    d:Ge/Patient/TransX  = 7.339062500000011 mm
```

```
    d:Ge/Patient/TransY  = -10.967187499999994 mm
    d:Ge/Patient/TransZ  = 16.25 mm
#=====================================================================#
#--- Scoring1
#=====================================================================#
    s:Sc/DoseOnCTGrid/Quantity = ”DoseToMedium”
    s:Sc/DoseOnCTGrid/Component = ”Patient”
    b:Sc/DoseOnCTGrid/OutputToConsole = ”False”
    s:Sc/DoseOnCTGrid/IfOutputFileAlreadyExists = ”Overwrite”
    s:Sc/DoseOnCTGrid/OutputType  = ”DICOM”
    b:Sc/DoseOnCTGrid/DICOMOutput32BitsPerPixel = ”False”
    b:Sc/DoseOnCTGrid/OutputAfterRun  = ”True”
    sv:Sc/DoseOnCTGrid/Report = 1 ”Sum”
    s:Sc/DoseOnCTGrid/OutputFile  = ”/home/erasmusmc.nl/051097/yartos
    /patients/Patient_Pt006Gr1/OUTPUT_1/Dose_scoring1_DICOM_phi1”
#=====================================================================#
#--- View
#=====================================================================#
    b:Gr/ViewA/Active = ”False” # defaults to ”True”
    b:Ts/PauseBeforeQuit = ”False”
```

Appendix E: 300 MeV treatment plans per patient for 9,18 and 36 beams

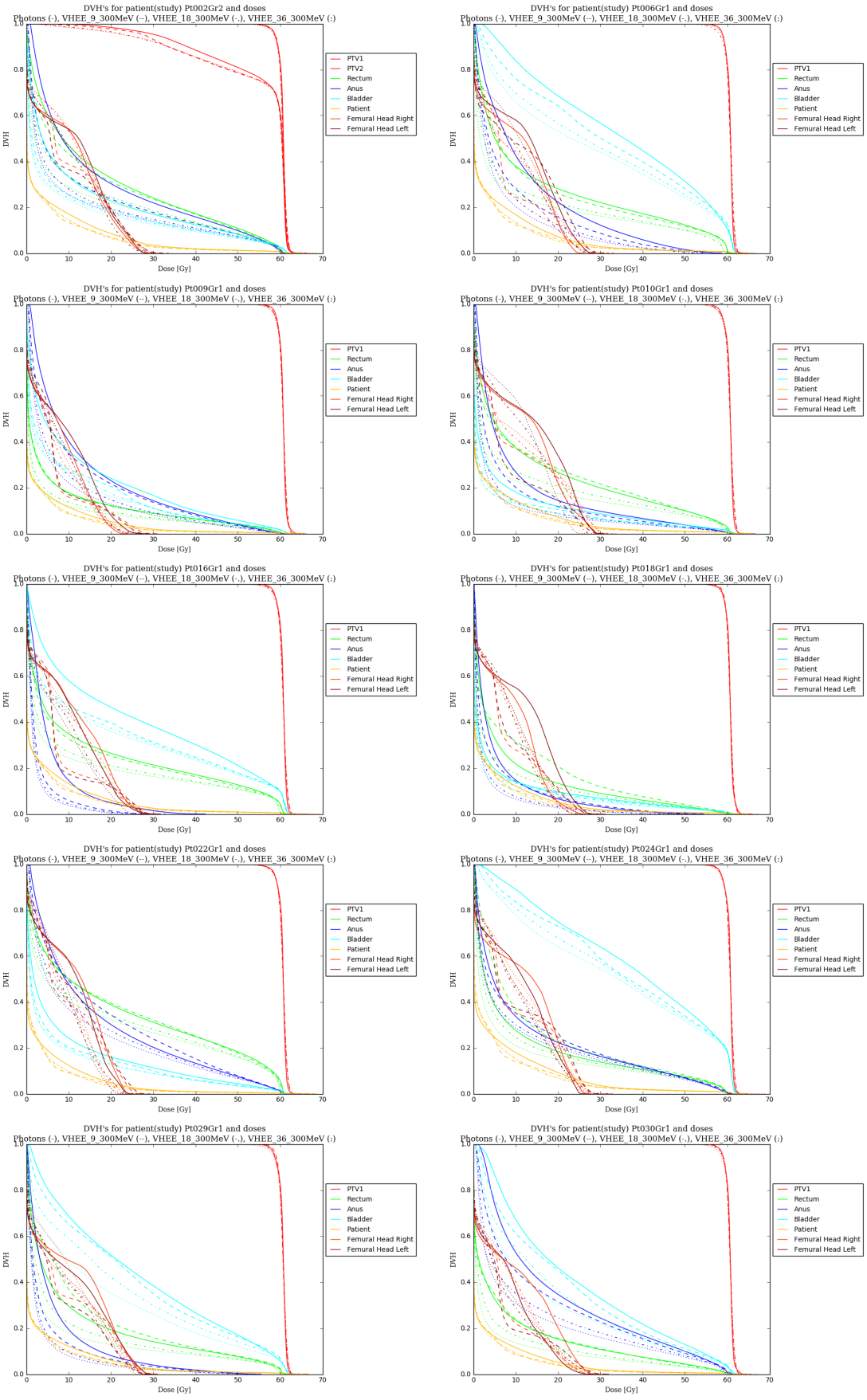

Figure E.1: Dose volume histograms per patient comparing photon treatment plan and the 9-18-36 beam treatment plans for 300 MeV. With grapsh of the PTV (red), bladder (light blue), anus (dark blue) and rectum (green).

Appendix F: 18 beam plans per patient for 200,300 and 400 MeV

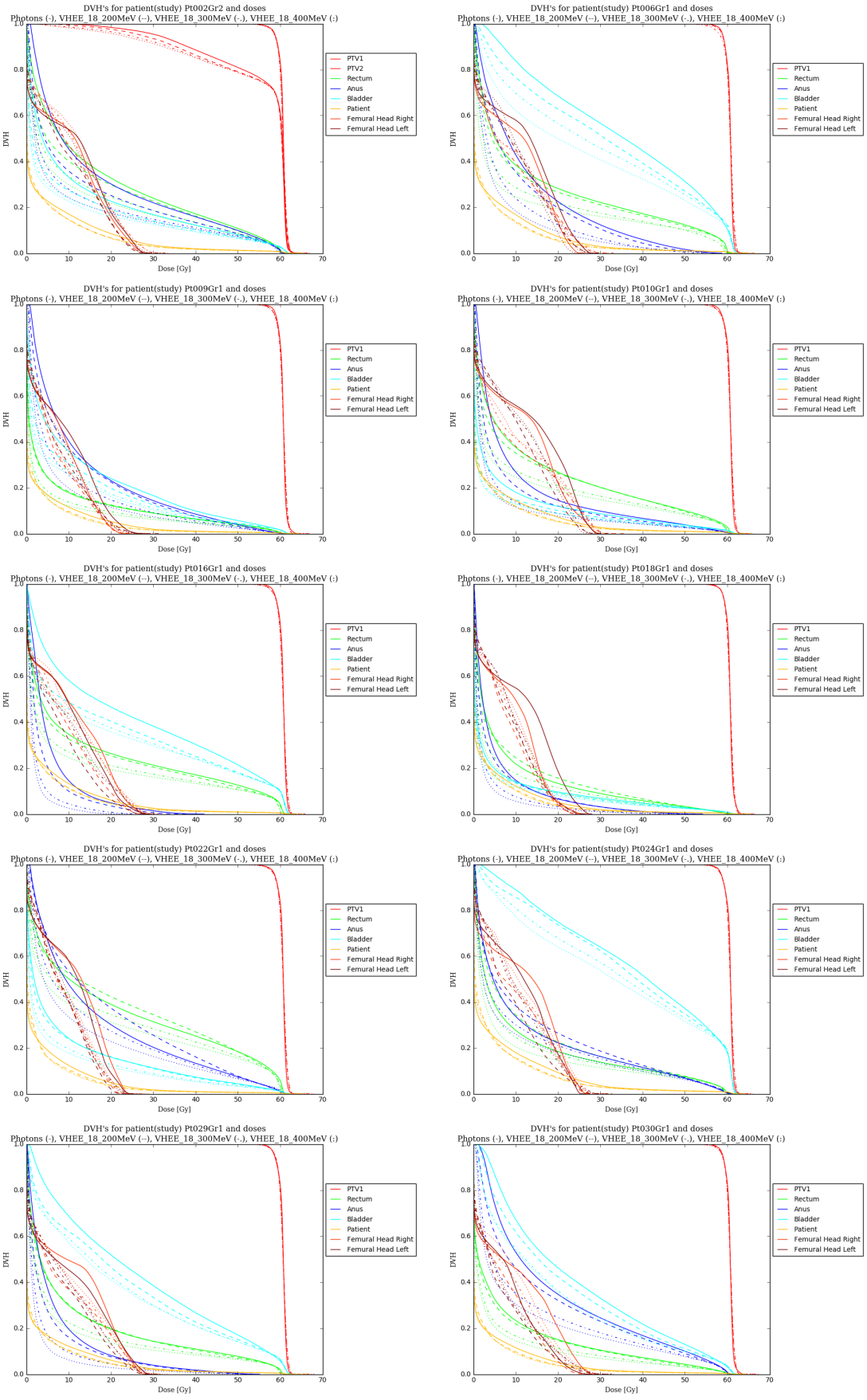

Figure F.1: Dose volume histograms per patient comparing photon treatment plan and the 200-300-400 MeV treatment plans for 18 beams. With grapsh of the PTV (red), bladder (light blue), anus (dark blue) and rectum (green).

Appendix G: Table of dosimetric values

Table G.1: Dose metrics comparing 23 beam IMRT with VHEE 9, 18 and 36 beam treatment plans for 200, 300 and 400 MeV. Table shows mean values for metrics with one standard deviation (n=10).Results are shown for PTV, rectum, anus, bladder, left femur head (LFH), right femur head (RFH) and the complete patient. T-tests have been performed between IMRT and VHEE treatment plans.

		IMRT	9 Beams 200 MeV	18 Beams 200 MeV	36 Beams 200 MeV	9 Beams 300 MeV	18 Beams 300 MeV	36 Beams 300 MeV	18 Beams 400 MeV	36 Beams 400 MeV
PTV	$V_{57Gy}(\%)$	99.9 ± 0.04	99.9 ± 0.02	99.9 ± 0.03	99.9 ± 0.03	99.9 ± 0.04	99.9 ± 0.04	99.8 ± 0.04	99.8 ± 0.08	99.7 ± 0.04
	$V_{64,2Gy}(\%)$	0.0	0.0	0.0	0.0	0.0	0.0	0.0	0.0	0.0
	$D_{0.001cc}(Gy)$	66.5 ± 0.5	65.9 ± 0.4	66.3 ± 0.3	67.1 ± 0.2	66.1 ± 0.5	66.7 ± 0.6	67.3 ± 0.4	66.8 ± 0.4	67.7 ± 0.3
	$D_{mean}(Gy)$	63.5 ± 0.3	63.4 ± 0.4	63.8 ± 0.3	64.3 ± 0.3	63.6 ± 0.5	64.2 ± 0.6	64.6 ± 0.4	64.3 ± 0.4	64.9 ± 0.3
	$CI_{95\%}$	1.10 ± 0.02	1.09 ± 0.02	1.09 ± 0.01	1.10 ± 0.02	1.09 ± 0.02	1.10 ± 0.02	1.11 ± 0.02	1.11 ± 0.02	1.12 ± 0.02
	$CI_{Riet95\%}$	0.89 ± 0.02	0.90 ± 0.01	0.90 ± 0.01	0.89 ± 0.01	0.90 ± 0.01	0.89 ± 0.02	0.88 ± 0.01	0.88 ± 0.01	0.88 ± 0.01
	$CI_{50\%}$	4.84 ± 0.27	4.30 ± 0.33	4.20 ± 0.27	4.28 ± 0.28	4.08 ± 0.31	4.05 ± 0.21	4.15 ± 0.30	3.97 ± 0.21	3.96 ± 0.25
Rectum	$D_{mean}(Gy)$	13.5 ± 4.4	17.1 ± 4.6	13.4 ± 4.3	11.9 ± 4.2	14.0 ± 3.9	11.1 ± 3.8	9.9 ± 3.7	10.0 ± 3.6	9.2 ± 3.4
	$V_{58Gy}(\%)$	6.5 ± 3.59	6.9 ± 3.65	6.2 ± 3.45	6.1 ± 3.34	6.4 ± 3.37	6.0 ± 3.30	6.0 ± 3.29	6.0 ± 3.30	6.0 ± 3.29
	$V_{50Gy}(\%)$	10.2 ± 4.81	11.8 ± 5.33	9.9 ± 4.85	9.3 ± 4.69	10.1 ± 4.55	8.8 ± 4.34	8.4 ± 4.22	8.3 ± 4.13	8.0 ± 4.03
Patient	$D_{mean}(Gy)$	4.1 ± 0.7	3.8 ± 0.6	3.7 ± 0.6	3.7 ± 0.6	3.6 ± 0.6	3.6 ± 0.7	3.6 ± 0.6	3.6 ± 0.7	3.5 ± 0.7
	$V_{3Gy}(\%)$	23.4 ± 2.98	24.3 ± 3.37	23.8 ± 3.25	23.6 ± 3.29	24.0 ± 3.32	23.5 ± 3.36	22.9 ± 3.31	23.1 ± 3.23	22.4 ± 3.33
	$V_{15Gy}(\%)$	10.2 ± 1.96	9.0 ± 1.70	8.3 ± 1.66	8.1 ± 1.69	8.3 ± 1.64	8.0 ± 1.75	7.8 ± 1.73	7.8 ± 1.75	7.7 ± 1.81
	$V_{30Gy}(\%)$	2.9 ± 0.73	2.3 ± 0.56	2.3 ± 0.60	2.4 ± 0.64	2.2 ± 0.54	2.3 ± 0.62	2.4 ± 0.64	2.3 ± 0.63	2.3 ± 0.67
Anus	$D_{mean}(Gy)$	12.4 ± 4.9	14.1 ± 6.1	11.4 ± 5.2	10.2 ± 4.8	10.6 ± 5.1	8.7 ± 4.5	8.0 ± 4.2	7.5 ± 4.1	7.0 ± 3.9
Bladder	$D_{mean}(Gy)$	20.1 ± 11.5	19.7 ± 11.6	18.2 ± 11.0	17.3 ± 10.6	18.0 ± 11.0	16.8 ± 10.5	15.8 ± 10.0	15.9 ± 9.9	15.2 ± 9.8
L.F.H.	$D_{0.001cc}(Gy)$	28.5 ± 1.5	28.2 ± 1.4	28.4 ± 2.0	27.9 ± 3.3	30.2 ± 1.2	29.1 ± 2.1	28.1 ± 2.2	28.8 ± 2.3	27.9 ± 3.2
R.F.H.	$D_{0.001cc}(Gy)$	27.8 ± 2.2	28.2 ± 1.7	28.0 ± 2.9	28.7 ± 3.2	30.1 ± 1.2	29.5 ± 3.1	28.6 ± 3.0	29.6 ± 2.8	28.3 ± 3.7

Table G.2: P - values of t-test comparing IMRT treatment plans and the VHEE treatment plans

		P - values							
		9 Beams 200 MeV	18 Beams 200 MeV-	36 Beams 200 MeV	9 Beams 300 MeV	18 Beams 300 MeV	36 Beams 300 MeV	18 Beams 400 MeV	36 Beams 400 MeV
PTV	$V_{57Gy}(\%)$	0.770	0.193	0.020	0.049	0.014	0.002	0.004	0.002
	$D_{0.001cc}(Gy)$	0.006	0.275	0.004	0.064	0.375	0.002	0.049	0.002
	$D_{mean}(Gy)$	0.375	0.064	0.002	0.625	0.004	0.002	0.004	0.002
	$CI_{95\%}$	0.064	0.232	0.695	0.432	0.695	0.131	0.160	0.037
	$CI_{Riet95\%}$	0.084	0.322	0.695	0.432	0.625	0.105	0.131	0.027
	$CI_{50\%}$	0.004	0.002	0.002	0.002	0.002	0.002	0.002	0.002
Rectum	$D_{mean}(Gy)$	0.002	0.695	0.004	0.375	0.002	0.002	0.002	0.002
	$V_{58Gy}(\%)$	0.004	0.006	0.004	1.000	0.002	0.002	0.002	0.002
	$V_{50Gy}(\%)$	0.002	0.105	0.002	0.695	0.002	0.002	0.002	0.002
Patient	$D_{mean}(Gy)$	0.002	0.002	0.002	0.002	0.002	0.002	0.002	0.002
	$V_{3Gy}(\%)$	0.020	0.105	0.432	0.037	0.625	0.131	0.322	0.014
	$V_{15Gy}(\%)$	0.002	0.002	0.002	0.002	0.002	0.002	0.002	0.002
	$V_{30Gy}(\%)$	0.002	0.002	0.002	0.002	0.002	0.002	0.002	0.002
Anus	$D_{mean}(Gy)$	0.020	0.160	0.010	0.014	0.002	0.002	0.002	0.002
Bladder	$D_{mean}(Gy)$	0.492	0.002	0.002	0.002	0.002	0.002	0.002	0.002
L.F.H.	$D_{0.001cc}(Gy)$	0.625	0.695	0.322	0.010	0.375	0.492	0.846	0.770
R.F.H.	$D_{0.001cc}(Gy)$	0.695	1.000	0.432	0.004	0.037	0.275	0.006	0.492

Bibliography

[1] M. Alber and Rembert Reemtsen. Intensity modulated radiotherapy treatment planning by use of a barrier-penalty multiplier method. *Optimization Methods and Software - OPTIM METHOD SOFTW*, 22:391–411, 06 2007. doi: 10.1080/10556780600604940.

[2] M. Bazalova, B. Qu, B. Palma, E. Hynning, B. Hardemark, P. G. Maxim, and B. W. Loo. Treatment-Planning Study for Very High-Energy Electron Beam Radiation Therapy: Integral Dose Reduction for Pediatric Patients. *International Journal of Radiation Oncology • Biology • Physics*, 90(1): S935–S936, September 2014. ISSN 0360-3016. doi: 10.1016/j.ijrobp.2014.05.2647. URL https://www.redjournal.org/article/S0360-3016(14)03298-2/abstract.

[3] Magdalena Bazalova Carter, Michael Liu, Bianey Palma, Michael Dunning, Doug McCormick, Erik Hemsing, Janice Nelson, Keith Jobe, Eric Colby, Albert C. Koong, Sami Tantawi, Valery Dolgashev, Peter G. Maxim, and Billy W. Loo. Comparison of film measurements and Monte Carlo simulations of dose delivered with very high-energy electron beams in a polystyrene phantom. *Medical Physics*, 42(4):1606–1613, 2015. ISSN 2473-4209. doi: 10.1118/1.4914371. URL https://aapm.onlinelibrary.wiley.com/doi/abs/10.1118/1.4914371.

[4] Magdalena Bazalova-Carter, Bradley Qu, Bianey Palma, Björn Hårdemark, Elin Hynning, Christopher Jensen, Peter G. Maxim, and Billy W. Loo. Treatment planning for radiotherapy with very high-energy electron beams and comparison of VHEE and VMAT plans: Treatment planning for VHEE radiotherapy. *Medical Physics*, 42(5):2615–2625, April 2015. ISSN 00942405. doi: 10.1118/1.4918923. URL http://doi.wiley.com/10.1118/1.4918923.

[5] MJ Berger, JS Coursey, MA Zucker, and J Chang. Stopping-power and range tables for electrons, protons, and helium ions, nist standard reference database 124, 2017.

[6] Sebastiaan Breedveld and Ben Heijmen. Data for trots–the radiotherapy optimisation test set. *Data in brief*, 12:143–149, 2017.

[7] Sebastiaan Breedveld, Pascal R. M. Storchi, Peter W. J. Voet, and Ben J. M. Heijmen. iCycle: Integrated, multicriterial beam angle, and profile optimization for generation of coplanar and noncoplanar IMRT plans. *Medical Physics*, 39(2):951–963, 2012. ISSN 2473-4209. doi: 10.1118/1.3676689. URL https://aapm.onlinelibrary.wiley.com/doi/abs/10.1118/1.3676689.

[8] Karl Kenneth Bush and Sergei F. Zavgorodni. IEC accelerator beam coordinate transformations for clinical Monte Carlo simulation from a phase space or full BEAMnrc particle source. *Australasian Physical & Engineering Sciences in Medicine*, 33:351–355, 2010. doi: 10.1007/s13246-010-0037-1.

[9] David S Chang, Foster D Lasley, Indra J Das, Marc S Mendonca, and Joseph R Dynlacht. Therapeutic ratio. In *Basic Radiotherapy Physics and Biology*, pages 277–282. Springer, 2014.

[10] Tom Depuydt. Proton therapy technology in the clinic, October 2017. URL http://www.icrp.org/docs/icrp2017/17%20Depuydt%20Presentation.pdf.

[11] C DesRosiers, V Moskvin, A F Bielajew, and L Papiez. 150-250 MeV electron beams in radiation therapy. *Physics in Medicine and Biology*, 45(7):1781–1805, July 2000. ISSN 0031-9155, 1361-6560. doi: 10.1088/0031-9155/45/7/306. URL http://stacks.iop.org/0031-9155/45/i=7/a=306?key=crossref.32c79da60619831e49a487ca7ceff192.

[12] Colleen DesRosiers, Vadim Moskvin, Minsong Cao, Chandrashekhar J. Joshi, and Mark Langer. Laser-plasma generated very high energy electrons in radiation therapy of the prostate. page 688109, San Jose, CA, February 2008. doi: 10.1117/12.761663. URL http://proceedings.spiedigitallibrary.org/proceeding.aspx?doi=10.1117/12.761663.

[13] T Fuchs, H Szymanowski, U Oelfke, Y Glinec, C Rechatin, J Faure, and V Malka. Treatment planning for laser-accelerated very-high energy electrons. *Physics in Medicine and Biology*, 54 (11):3315–3328, June 2009. ISSN 0031-9155, 1361-6560. doi: 10.1088/0031-9155/54/11/003. URL http://stacks.iop.org/0031-9155/54/i=11/a=003?key=crossref.65c01513edc51d9c997048b30424d3fb.

[14] H. M. Garnica-Garza. Influence of the electron energy and number of beams on the absorbed dose distributions in radiotherapy of deep seated targets. *Applied Radiation and Isotopes*, 94: 101–108, December 2014. ISSN 0969-8043. doi: 10.1016/j.apradiso.2014.07.018. URL http://www.sciencedirect.com/science/article/pii/S0969804314002978.

[15] Y. Glinec, J. Faure, V. Malka, T. Fuchs, H. Szymanowski, and U. Oelfke. Radiotherapy with laser-plasma accelerators: Monte Carlo simulation of dose deposited by an experimental quasi-monoenergetic electron beam. *Medical Physics*, 33(1):155–162, 2006. ISSN 2473-4209. doi: 10.1118/1.2140115. URL https://aapm.onlinelibrary.wiley.com/doi/abs/10.1118/1.2140115.

[16] John CP Heggie, Neil A Liddell, and Kieran P Maher. *Applied imaging technology*. St. Vincent's Hospital, 2001.

[17] Andrea Holt, Corine van Vliet-Vroegindeweij, Anton Mans, José S Belderbos, and Eugène MF Damen. Volumetric-modulated arc therapy for stereotactic body radiotherapy of lung tumors: a comparison with intensity-modulated radiotherapy techniques. *International Journal of Radiation Oncology* Biology* Physics*, 81(5):1560–1567, 2011.

[18] Gospodarowicz MK Jaffray DA. *Cancer: Disease Control Priorities, Third Edition (Volume 3), Chapter 14*, volume 3. Washington (DC): The International Bank for Reconstruction and Development / The World Bank, 11 2015.

[19] Christian P Karger. Biological models in treatment planning. In *New Technologies in Radiation Oncology*, pages 221–235. Springer, 2006.

[20] K. Kokurewicz, E. Brunetti, G. H. Welsh, S. M. Wiggins, M. Boyd, A. Sorensen, A. J. Chalmers, G. Schettino, A. Subiel, C. DesRosiers, and D. A. Jaroszynski. Focused very high-energy electron beams as a novel radiotherapy modality for producing high-dose volumetric elements. *Scientific Reports*, 9(1):1–10, July 2019. ISSN 2045-2322. doi: 10.1038/s41598-019-46630-w. URL https://www.nature.com/articles/s41598-019-46630-w.

[21] A Lagzda and R M Jones. Relative Insensitivity to Inhomogeneities on Very High Energy Electron Dose Distributions. page 4, 2017.

[22] Agnese Lagzda. Vhee radiotherapy studies at clara and clear facilities. *Ann Arbor*, 1001:48106–1346, 2019.

[23] Agnese Lagzda, Adam Aitkenhead, Roberto Corsini, Wilfrid Farabolini, Roger Jones, Karen Kirkby, Ranald MacKay, and Marcel Van Herk. Very-High Energy Electron (VHEE) Studies at CERN's CLEAR User Facility. *Proceedings of the 9th Int. Particle Accelerator Conf.*, IPAC2018:4 pages, 3.662 MB, 2018. doi: 10.18429/jacow-ipac2018-mopml023. URL http://jacow.org/ipac2018/doi/JACoW-IPAC2018-MOPML023.html.

[24] R Leroy, N Benahmed, F Hulstaert, F Mambourg, N Fairon, L Van Eycken, N Benahmed, F Hulstaert, F Mambourg, N Fairon, et al. Hadron therapy in children–an update of the scientific evidence for 15 paediatric cancers. *Health Technology Assessment (HTA). KCE Reports*, 235, 2015.

[25] Eugene P. Lief, Anders Larsson, and John L. Humm. Electron dose profile shaping by modulation of a scanning elementary beam. *Medical Physics*, 23(1):33–44, 1996. ISSN 2473-4209. doi: 10.1118/1.597786. URL https://aapm.onlinelibrary.wiley.com/doi/abs/10.1118/1.597786.

[26] O. Lundh, C. Rechatin, J. Faure, A. Ben□Ismaïl, J. Lim, C. De Wagter, W. De Neve, and V. Malka. Comparison of measured with calculated dose distribution from a 120-MeV electron beam from a laser-plasma accelerator. *Medical Physics*, 39(6Part1):3501–3508, 2012. ISSN 2473-4209. doi: 10.1118/1.4719962. URL https://aapm.onlinelibrary.wiley.com/doi/abs/10.1118/1.4719962.

[27] Victor Malka, Jérôme Faure, Yannick Glinec, Clément Rechatin, Thomas Fuchs, Uwe Oelfke, and Hannitra Szymanowski. Medical applications with electron beam generated by laser plasma accelerators. In *Commercial and Biomedical Applications of Ultrafast Lasers VIII*, volume 6881, page 68810B. International Society for Optics and Photonics, March 2008. doi: 10.1117/12.763842. URL https://www.spiedigitallibrary.org/conference-proceedings-of-spie/6881/68810B/Medical-applications-with-electron-beam-generated-by-laser-plasma-accelerators/10.1117/12.763842.short.

[28] Victor Malka, Jérôme Faure, and Yann A. Gauduel. Ultra-short electron beams based spatio-temporal radiation biology and radiotherapy. *Mutation Research/Reviews in Mutation Research*, 704(1):142–151, April 2010. ISSN 1383-5742. doi: 10.1016/j.mrrev.2010.01.006. URL http://www.sciencedirect.com/science/article/pii/S1383574210000104.

[29] Peter G. Maxim, Sami G. Tantawi, and Billy W. Loo. PHASER: A platform for clinical translation of FLASH cancer radiotherapy. *Radiotherapy and Oncology*, June 2019. ISSN 0167-8140. doi: 10.1016/j.radonc.2019.05.005. URL http://www.sciencedirect.com/science/article/pii/S0167814019304049.

[30] William F Morgan and Marianne B Sowa. Effects of ionizing radiation in nonirradiated cells. *Proceedings of the National Academy of Sciences*, 102(40):14127–14128, 2005.

[31] Kazuhisa Nakajima, Jianjun Yuan, Liming Chen, and Zhengming Sheng. Laser-Driven Very High Energy Electron/Photon Beam Radiation Therapy in Conjunction with a Robotic System. *Applied Sciences*, 5(1):1–20, March 2015. doi: 10.3390/app5010001. URL https://www.mdpi.com/2076-3417/5/1/1.

[32] Bianey Palma, Magdalena Bazalova-Carter, Björn Hårdemark, Elin Hynning, Bradley Qu, Billy W. Loo, and Peter G. Maxim. Assessment of the quality of very high-energy electron radiotherapy planning. *Radiotherapy and Oncology*, 119(1):154–158, April 2016. ISSN 0167-8140. doi: 10.1016/j.radonc.2016.01.017. URL http://www.sciencedirect.com/science/article/pii/S0167814016000487.

[33] Lech Papiez, Colleen DesRosiers, and Vadim Moskvin. Very High Energy Electrons (50 – 250 MeV) and Radiation Therapy. *Technology in Cancer Research & Treatment*, 1(2):105–110, April 2002. ISSN 1533-0346, 1533-0338. doi: 10.1177/153303460200100202. URL http://journals.sagepub.com/doi/10.1177/153303460200100202.

[34] Ianik Plante and Francis A Cucinotta. Cross sections for the interactions of 1 ev–100 mev electrons in liquid water and application to monte-carlo simulation of hze radiation tracks. *New Journal of Physics*, 11(6):063047, 2009.

[35] ERVIN B Podgorsak. External photon beams: Physical aspects. *Radiation Oncology Physics: A handbook for teachers and students'. Vienna: IAEA*, page 169, 2005.

[36] Ervin B Podgoršak. Interaction of charged particles with matter. In *Compendium to Radiation Physics for Medical Physicists*, pages 299–386. Springer, 2014.

[37] Julie A Reisz, Nidhi Bansal, Jiang Qian, Weiling Zhao, and Cristina M Furdui. Effects of ionizing radiation on biological molecules—mechanisms of damage and emerging methods of detection. *Antioxidants & redox signaling*, 21(2):260–292, 2014.

[38] Uwe Schneider and Roger Hälg. The impact of neutrons in clinical proton therapy. *Frontiers in Oncology*, 5:235, 2015.

[39] Emil Schüler, Kjell Eriksson, Elin Hynning, Steven L. Hancock, Susan M. Hiniker, Magdalena Bazalova□Carter, Tony Wong, Quynh-Thu Le, Billy W. Loo, and Peter G. Maxim. Very high-energy electron (VHEE) beams in radiation therapy; Treatment plan comparison between VHEE, VMAT, and PPBS. *Medical Physics*, 44(6):2544–2555, 2017. ISSN 2473-4209. doi: 10.1002/mp.12233. URL https://aapm.onlinelibrary.wiley.com/doi/abs/10.1002/mp.12233.

[40] Gloria Spirou Orchard, I. Yavin, Matthew Weel, Andrew Vorozcovs, A. Kumarakrishnan, P. Battle, and R. Swanson. A high-speed-modulated retro-reflector for lasers using an acousto-optic modulator. *Canadian Journal of Physics - CAN J PHYS*, 81:625–638, apr 2003. doi: 10.1139/p03-047.

[41] A Subiel, V Moskvin, G H Welsh, S Cipiccia, D Reboredo, P Evans, M Partridge, C DesRosiers, M P Anania, A Cianchi, A Mostacci, E Chiadroni, D Di Giovenale, F Villa, R Pompili, M Ferrario, M Belleveglia, G Di Pirro, G Gatti, C Vaccarezza, B Seitz, R C Isaac, E Brunetti, S M Wiggins, B Ersfeld, M R Islam, M S Mendonca, A Sorensen, M Boyd, and D A Jaroszynski. Dosimetry of very high energy electrons (VHEE) for radiotherapy applications: using radiochromic film measurements and Monte Carlo simulations. *Physics in Medicine and Biology*, 59(19): 5811–5829, October 2014. ISSN 0031-9155, 1361-6560. doi: 10.1088/0031-9155/59/19/5811. URL http://stacks.iop.org/0031-9155/59/i=19/a=5811?key=crossref.c597108f1224d85d4a719ea6d27427c7.

[42] Anna Subiel, Vadim Moskvin, Gregor H. Welsh, Silvia Cipiccia, David Reboredo, Colleen DesRosiers, and Dino A. Jaroszynski. Challenges of dosimetry of ultra-short pulsed very high energy electron beams. *Physica Medica*, 42:327–331, October 2017. ISSN 1120-1797. doi: 10.1016/j.ejmp.2017.04.029. URL http://www.sciencedirect.com/science/article/pii/S1120179717301151.

[43] Manfei Xu, Drew Fralick, Julia Z Zheng, Bokai Wang, Xin M Tu, and Changyong Feng. The differences and similarities between two-sample t-test and paired t-test. *Shanghai archives of psychiatry*, 29(3):184, 2017.

[44] C Yeboah and G A Sandison. Optimized treatment planning for prostate cancer comparing IMPT, VHEET and 15 MV IMXT. *Physics in Medicine and Biology*, 47(13):2247–2261, July 2002. ISSN 00319155. doi: 10.1088/0031-9155/47/13/305. URL http://stacks.iop.org/0031-9155/47/i=13/a=305?key=crossref.18fb83aa96f675543c4013255ac442c4.

[45] C Yeboah, G A Sandison, and V Moskvin. Optimization of intensity-modulated very high energy (50–250 MeV) electron therapy. *Physics in Medicine and Biology*, 47(8): 1285–1301, April 2002. ISSN 0031-9155, 1361-6560. doi: 10.1088/0031-9155/47/8/305. URL http://stacks.iop.org/0031-9155/47/i=8/a=305?key=crossref.c4febbd4ac189ffa1901c07519019ad3.

[46] Seung Hoon Yoo, Byung Jun Min, Sungho Cho, Eun Ho Kim, Jeong Hoon Park, Won-Gyun Jung, Geun Beom Kim, Kum Bae Kim, Jaehoon Kim, Hojin Jeong, Kitae Lee, and Sung Yong Park. Dosimetric properties of plasma density effects on laser-accelerated VHEE beams using a sharp density-transition scheme. *Journal of the Korean Physical Society*, 70(1):66–74, January 2017. ISSN 0374-4884, 1976-8524. doi: 10.3938/jkps.70.66. URL http://link.springer.com/10.3938/jkps.70.66.